Politecnico di Torino

Politecnico di Torino

Master of science in Energy and Nuclear Engineering

CFD analysis of a thermocline molten salt energy storage for CSP plants hybridized with an electric microwave heating system

Supervisors:

Prof. Roberto Zanino

Dr. Mehdi Shokrnia

Dr. Mattia Cagnoli

Candidate:

Francesco Prato

Academic year 2023-2024

Summary

Acronyms

BTM	Tank bottom
CAD	Computer-aided design
CFD	Computational Fluid Dynamics
CSP	Concentrated Solar Power
DNI	Direct Normal Irradiation
ENEA	Agenzia nazionale per le nuove tecnologie, l'energia e lo sviluppo economico sostenibile
HTF	Heat Transfer Fluid
IEA	International Energy Agency
MC	Microchannels
MS	Molten Salt
MW	Microwaves
NZE	Net Zero Emissions
ORC	Organic Rankine Cycle
PCM	Phase Change Material
PV	Photovoltaic
SM	Solar Multiple
TD	Temperature Difference
TES	Thermal Energy Storage
TOP	Tank Top
TS	Temperature Stratification

Abstract

The aim of this work is to study, through computational fluid dynamics (CFD) models, the charge transient of a thermocline sensible thermal storage for concentrated solar power plants (CSP). A thermocline storage is characterized by the stratification of the temperature inside the tank, in which the upper part is at a higher temperature than the lower part. This solution allows to avoid the classic double tank configuration used for CSP applications, in which the two tanks contain the fluid at two different constant temperatures. The thermocline storage allows, therefore, to supply the cold fluid to the solar field and the hot fluid to the power plant using a single tank. The choice to study this type of thermal storage derives from the continuation of several studies carried out in previous years by the Agenzia nazionale per le nuove tecnologie, l'energia e lo sviluppo economico sostenibile (ENEA).

The model developed by ENEA consists of a tank with a central channel, at the ends of which there are two heat exchangers, used for charging and discharging the storage. Inside the heat exchangers pipes the heat transfer fluids flow. In this work, it was decided to develop a model in which the charging phase is carried out thanks to an additional device, which uses microwaves (MW) to irradiate and heat up the storage medium (molten salt). Microwaves represent a very efficient method for heating a fluid starting from electrical energy. This aspect allows for a hybridization between CSP plants and photovoltaic (PV) plants. In fact, the idea is precisely to recover the surplus energy (in the central hours of the day) of the PV plants and store it to be used later when the demand increases (generally, during the evening). In this work, after having provided the reader with the theoretical basis regarding CSP plants, thermal storage and microwave heating, the various steps in the construction of the model are explained in detail. First of all, the model developed by ENEA is briefly explained, which represents the basis for the subsequent models. Then, the geometry, the physics of the simulation, the boundary conditions and the mesh generation are presented. The models were built using the CAD *Solidworks* software, while the fluid dynamic simulations were performed using the *Simcenter STAR-CCM+* software.

The results are divided into three parts. In the first part, simulations of the charge transient were performed for two different configurations, A and B, which differ in the way in which the microwaves are discharged into the fluid. These simulations led to inadequate results regarding the temperature stratification. Since the poor stratification was seen to be caused by the excessive flow rate circulating in the channel, it was decided to make some changes to improve the performance. The first is the introduction of a “fan interface” that simulates the operation of an impeller inside the channel, to regulate the flow rate. This solution also proved to be inefficient. The second solution undertaken is the introduction of microchannels in the central channel, in order to create concentrated pressure drops, hindering the passage of the fluid. This solution has led to satisfactory results, thanks to a

better stratification of the temperature and an adequate temperature difference between the upper and lower part of the tank.

PART 1

The first part of this thesis provides a theoretical overview of the main topics covered in this thesis. In particular, the principles of Concentrated Solar Power (CSP), sensible energy storage and microwave heating technologies are explained. This first part is intended to facilitate the understanding of the second part of the thesis, which is an experimental study based on computational fluid dynamics (CFD) of a microwave-heated thermocline thermal energy storage for CSP plants.

1.1 Introduction

The aim of this work is the fluid dynamics study of a thermocline thermal storage used to store thermal energy in concentrated solar power (CSP) plants. The purpose of a thermal storage is to store energy for a certain period for later use. CSP plants are particularly suitable for the installation of thermal storage, since they produce heat at high temperatures. In general, the heat produced by CSP plants is used to produce electricity on the spot. However, in case, at certain times of the day, there is an excessive production compared to the demand, the energy can be stored and used when the demand increases.

Unlike the standard use of thermal storage, the subject of this thesis presents some additional innovative elements. In fact, the developed thermal energy storage (TES) has the possibility of being loaded both through conventional thermal energy from CSP plants and through electrical energy from photovoltaic (PV) plants. This choice is mainly due to the need to store, during the central hours of the day, the energy produced by PV panels that exceeds demand. In fact, as the spread of photovoltaic panels increases, the phenomenon of “curtailment”, the deliberate reduction of energy production below the achievable value, will become increasingly widespread. Thanks to TES, excess energy can be stored and used later, when demand increases and solar radiation is reduced or absent. Furthermore, an innovative element of this project concerns the method used to discharge energy into storage. The most widespread technology to discharge electrical energy consists of using thermal resistances, in which wires are crossed by electric current, to produce thermal energy by the Joule effect. However, it was decided, for reasons that will be analyzed later, to use an innovative method, the use of microwaves. Microwaves are generated using electrical energy from PV systems and discharge thermal energy into the storage medium by oscillating its molecules/ions.

1.1 Introduction

The reasons for which it was decided to undertake this project are mainly aimed at addressing the rapid and important changes that the energy sector is facing to reduce its environmental impact. In fact, in 2016, 195 members of the *United Nations Framework Convention on Climate Change* (UNFCCC) signed the agreement known as "Paris Agreement", which sets as its main objective to reduce greenhouse gas emissions so that the average temperature of the Earth's surface remains well below 2°C above pre-industrial times. Furthermore, it was decided, preferably, not to exceed 1.5°C to avoid the most serious effects of climate change.

In the document released by the *International Energy Agency* (IEA) "Net Zero Roadmap: A Global Pathway to Keep the 1.5 °C Goal in Reach" (IEA, 2023), a scenario is proposed, called "Net zero emissions scenario" (NZE), which provides the measures necessary to achieve the objectives of the Paris Agreement, reaching, for the energy sector, zero net carbon dioxide emissions by 2050. In the field of electricity production, the planned interventions can be grouped into the following macro-categories:

- Tripling of the installed capacity of renewable energy by 2030 compared to the levels of 2022, when the capacity was approximately 3600 GW. In 2030, electricity production from renewable sources will represent 60% of the total, while in 2050 90%.
- Doubling investments in the electricity transmission and distribution network by 2030.
- Reduction of 95% of the use of fossil fuels for electricity production by 2040, eliminating the use of coal.
- More than double installed nuclear capacity by 2050.

The following graph shows the projections of electricity production shares for each energy source for the NZE scenario assumed by IEA:

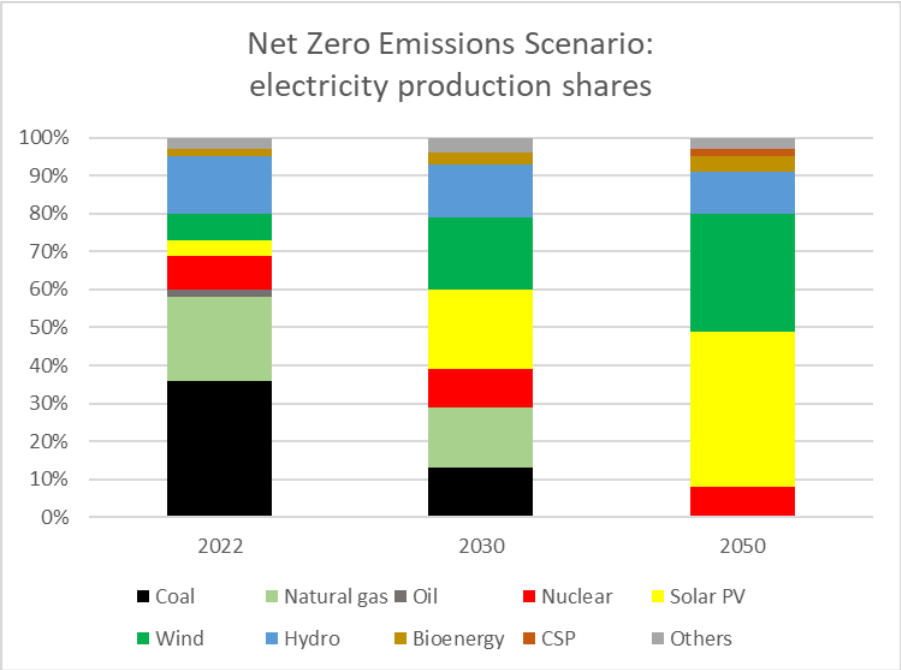

Figure 1 - NZE scenario: electrity production shares by energy source

From the graph, in 2022, electricity produced from fossil fuels constituted 61% of the total and the main source was still coal. Renewables in 2022 produced around 30% of the total, thus reaching a considerable share. Among renewables, half of the electricity was produced thanks to hydroelectric plants. According to the NZE scenario, the share of renewables will reach 59% in 2030 and 90% in 2050. On the contrary, fossil fuels will constitute 29% of the total in 2030 until reaching 0% in 2050. Nuclear will remain approximately stable, with a production of around 9%. Electricity produced by photovoltaics is estimated at around 41% of the total in 2050, while from concentrated solar only 2%.

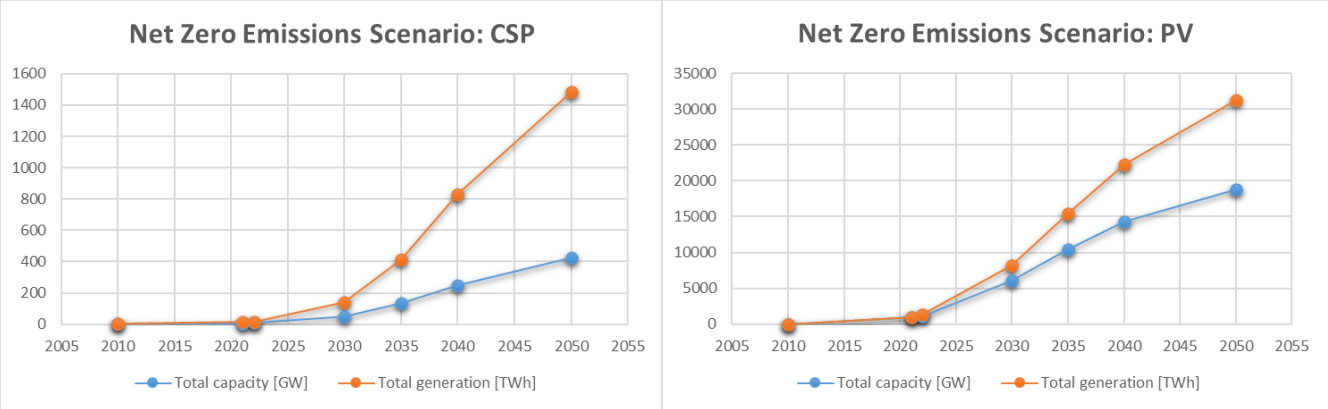

Figure 2 - NZE scenario: PV and CSP capacity and generation by 2050

For solar electricity generation technologies, i.e. PV and CSP, IEA proposes the following generation and installed capacity projections for 2050:

As it can be seen, the scale of values is very different for the two technologies, with PV remaining clearly the dominant solar technology in the future. However, a significant increase in CSP installations is also expected, with an increase of almost 7 times in installed capacity in 2030 compared to 2022.

1.2 Concentrated solar power

1.2.1 Overview

In this section, we would like to present the technology known as "Concentrated Solar Power", which makes it possible to produce electrical energy by concentrating in a receiver the direct solar radiation falling on a very large area covered by special mirrors. In the receiver, the concentrated solar radiation is used to heat a heat transfer fluid (HTF). Subsequently, the heat transported by the HTF is used directly or indirectly to produce mechanical energy through a conventional thermodynamic cycle, i.e. a steam Rankine cycle. The mechanical energy produced by the steam turbines is then transformed into electrical energy thanks to a generator.

There are four technologies for producing concentrated solar energy: parabolic trough, solar tower, linear Fresnel and parabolic dish. The parabolic trough technology represents the majority of the market, resulting in approximately 81% of the installed capacity (World Bank, 2021). The remaining part of the installed capacity is mainly made up of solar towers.

The main parameter for evaluating the economic feasibility of a CSP plant in a certain location is the direct normal irradiation (DNI), i.e. the amount of direct radiation that strikes a surface normal to the rays in a given period of time. In general, economic feasibility is evaluated with a minimum of 1900-2100 $\frac{kWh}{m^2}$ per year. In the following figure, the worldwide DNI levels are shown:

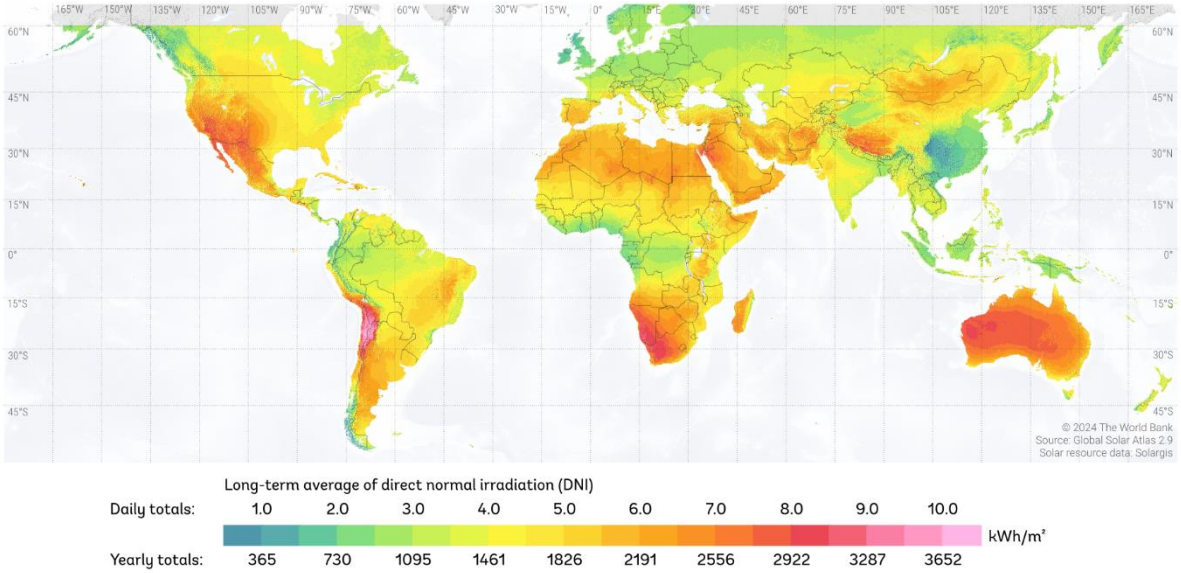

Figure 3 - Direct Normal Irradiation (ESMAP, 2024)

In general, arid or semi-arid areas are the most suitable for the installation of CSP plants, places where precipitations are rare, the sky is generally free of clouds and aerosols. In particular, the best levels of DNI are found in Chile and Peru, followed by Australia, Southern Africa, Western United States, Middle East and North Africa, Southern China.

CSP plants, although they are a valid alternative to solar PV, represent a minority share of the total power installed by solar energy. In fact, the global installed capacity of CSP plants was 6.88 GW in 2023, while the installed PV capacity was 1411 GW. The leading countries for CSP installed capacity are Spain (2304 MW), USA (1480 MW), China (570 MW), Morocco (540 MW), South Africa (500 MW) (IRENA, 2024).

In the following, the main characteristics related to solar radiation and CSP energy production technologies are briefly presented. The information provided in the following in this chapter has been obtained from (Lovegrove K., 2012) and (Günther M., 2011)

1.2.2 Solar radiation

In this section, we will explain the basic concepts of solar radiation, which is the primary source of energy used in CSP plants.

The Sun is the primary source of energy for all terrestrial activities. In fact, any renewable or non-renewable energy source used on Earth is the result of a transformation of solar energy into other forms of energy. The thermal and electromagnetic energy generated by the Sun is produced thanks to nuclear fusion reactions that constantly occur inside the nucleus, in which 4 protons fuse releasing a helium nucleus, 2 neutrinos and 2 positrons. The fusion process results in a mass defect, releasing energy according to the well-known formula $E = mc^2$, where c is the speed of light and m is the mass that is transformed into energy. Every second, inside the Sun 4.3 billion kg are transformed into energy, producing a power equal to $3.85 * 10^{26}\ W$.

The energy produced inside the Sun's core is released through radiative energy, of which a small part is radiation from matter and the majority is electromagnetic radiation. The electromagnetic radiation emitted by the Sun, called "solar spectrum", is very similar to the radiation emitted by a black body at 5777 K. The black body is a body that absorbs all the radiation that strikes it, without transmission or reflection. Such a body is not present in nature, but some bodies come very close to being considered black bodies. The emission spectrum of a black body, described by the black body law formulated by Max Planck, has temperature as its fundamental parameter. The radiation emitted by the black body is called thermal radiation and has a continuous spectrum as the wavelength varies. The total radiation emitted by a black body at a certain temperature is the area under the spectrum curve and is quantitatively calculated thanks to the Stefan-Boltzmann law, whose formula is:

$$P = A\sigma T^4\ [W] \qquad (1)$$

Where A is the body surface area and $\sigma = 5.67 * 10^{-8}\frac{W}{m^2K^4}$ is the Stefan-Boltzmann constant. The solar spectrum, as mentioned, is similar in shape to the spectrum of a black body, although not perfectly coinciding. The temperature of 5777 K is commonly considered because it allows for the equivalence between the real radiative power of the Sun and that of the black body. Most of the solar radiation is found in the visible light portion, while smaller portions are emitted in the ultraviolet and infrared ranges.

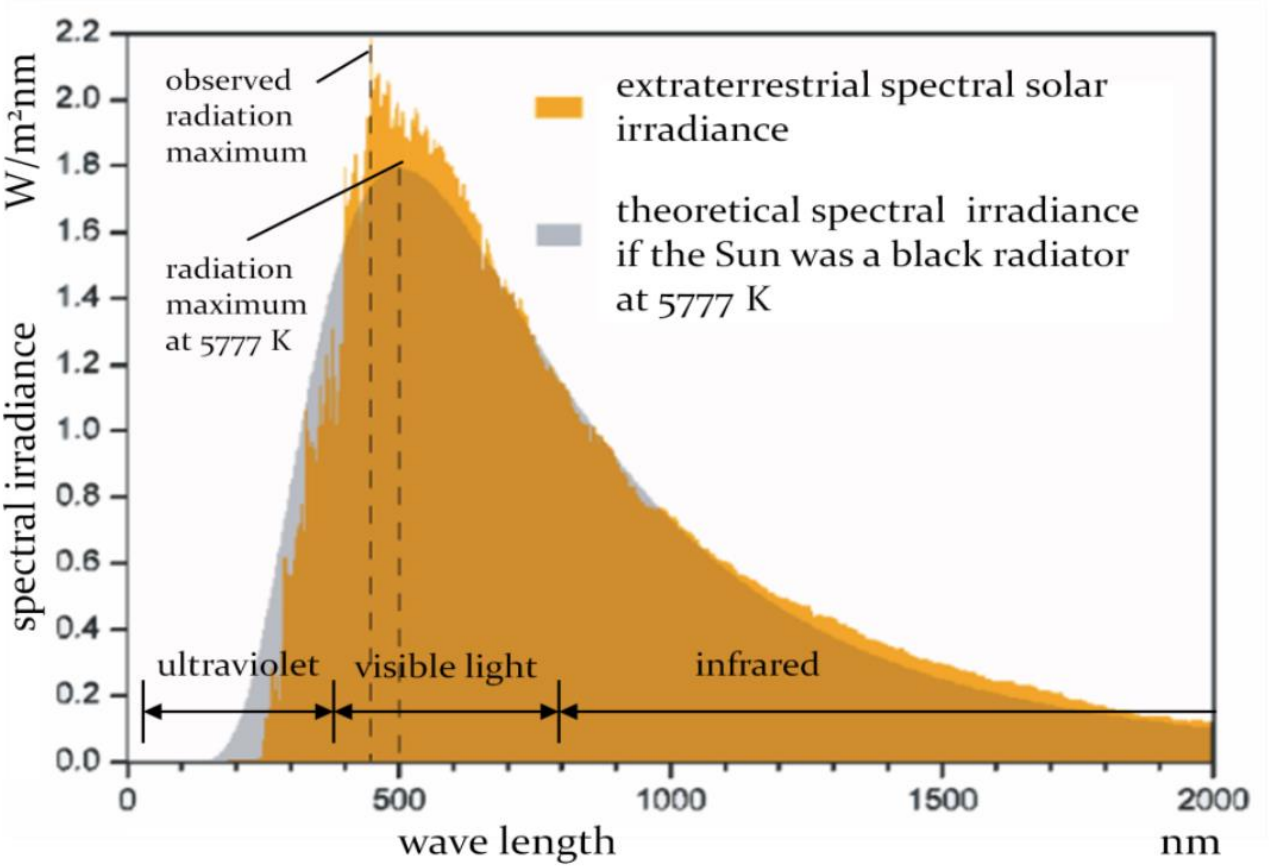

Figure 4 – Extraterrestrial spectral solar irradiance (Deutsches Zentrum für Luft- und Raumfahrt)

Despite the enormous amount of energy emitted by the Sun, only a small amount of it reaches the Earth. Furthermore, only a portion of the energy that reaches the Earth actually reaches the ground, due to losses in the atmosphere.

The power emitted by the Sun is emitted in all directions and is distributed over a larger surface area as one moves away from the source. For this reason, it is useful to define a quantity called the "solar constant". This quantity represents the power per unit of surface area that reaches the Earth's atmosphere. This quantity is nearly constant and depends on the temperature of the Sun (in particular, of the photosphere, one of the outermost layers), the size of the Sun and the distance between the Sun and the Earth. The power emitted is constant on every spherical surface with the Sun at its centre. Therefore, the irradiance, or power per unit of surface area, that reaches the top of the atmosphere is given by the total power emitted by the Sun divided by the surface area of the sphere with a radius r_{SE} equal to the distance between the Sun and the Earth, according to the formula:

$$G_{sc} = \frac{P_s}{4\pi r_{SE}^2} = 1367\ W/m^2 \qquad (2)$$

Where P_s is total power emitted by the Sun, calculated previously. G_{sc} is the incident irradiance on a surface positioned at the atmosphere top and perpendicular to the rays. This value is the average along the year, since the irradiance varies every day, mainly because of the non-circular Earth's orbit around the Sun.

Although on average the amount of power that reaches the Earth is given by the solar constant, a part of it is lost in extinction processes in the atmosphere. There are two types of extinction processes (i.e. the attenuation of radiation by atmospheric agents): absorption and scattering. In the first case, the particles present in the atmosphere, such as ozone or carbon dioxide, absorb the radiation in certain spectral ranges. In the second case, the radiation is deviated by particles encountered along the path, such as molecules or dust. Scattering prevents a part of the radiation from directly reaching the Earth's surface. This part of the radiation is called diffuse radiation. The scattering phenomenon is divided into two components: Rayleigh-scattering and Mie-scattering. In the first case, the radiation is deviated by particles with dimensions smaller than the wavelength, i.e. small molecules or atoms. This type of scattering depends exclusively on the so-called "air mass". The air mass is an index that quantifies the optical path of the radiation directed through the atmosphere. The longer the radiation path, the greater the attenuation. This index is given by the ratio between the actual path of the radiation to reach a point and the path it would take if the Sun were at its zenith.
In the second case, scattering is caused by particles with a diameter greater than the wavelength of the radiation, such as water drops, ice crystals. This type of phenomenon is mainly due to atmospheric conditions such as pollution, fog, clouds.

Therefore, the radiation that reaches the Earth's surface can be divided into two components: direct and diffuse. CSP systems, unlike photovoltaic systems, can only use direct radiation. In fact, diffuse radiation, being non-directional, cannot be concentrated. Finally, in the case in which we take into consideration the radiation that reaches a certain surface (such as the reflective surfaces of CSP systems) there is a third component, reflected radiation. However, this too, being non-directional, cannot be used in this type of system.

The last aspect that we want to discuss in this section concerns the limits to the concentration of radiation. The principle of concentration of radiation is due to the geometric properties of the parabola. In fact, the parabola always has a point, so that any ray hitting the parabolic mirror with a direction parallel to the axis is reflected at this point, called the focal point. In the case of mirrors, which are three-dimensional, the focal point can take the form of a line or a point.

From the geometric study of such concentration systems, physical limits to the concentration of radiation can be found. Before proceeding, it is appropriate to define the "concentration ratio", that is, the ratio between the radiation after concentration and the

radiation before concentration. This ratio can be approximated to the ratio between the aperture area, i.e. the area in which the radiation is collected, and the minimum area in which the radiation is reflected. Considering that the radiation is reflected in an absorber that only covers the Sun image, the concentration ratio can be expressed as:

$$C = \frac{Aperture\ area}{Absorber\ area} \tag{3}$$

Although one might think that the Sun's image could be a dimensionless point and the concentration ratio could assume infinite values, in reality, since the radiation does not reach the ground through perfectly parallel rays, the Sun's image occupies a certain area and not a point. Therefore, there are limits to the concentration ratio. It is possible to demonstrate that, in the case of systems with perfect reflectivity of the mirrors, perfect transmission of the receiver and in which the radiation extinction processes are zero, the concentration limits are the following:

$$C_{max,point} = 46200 \tag{4}$$

$$C_{max,line} = 215 \tag{5}$$

This limit is valid for any system, regardless of geometry. However, in the more specific case where parabolic mirrors are used, the concentration limits are reduced to:

$$C_{max,point} = 11550 \tag{6}$$

$$C_{max,line} = 107.5 \tag{7}$$

1.2.3 Technologies

There are four main CSP technologies: parabolic trough, solar tower, linear Fresnel and parabolic dish. Parabolic troughs and linear Fresnel concentrate the radiation in a line, while the other two technologies concentrate it in a point. After the picture showing the main components of these technologies, the main characteristics are briefly described below.

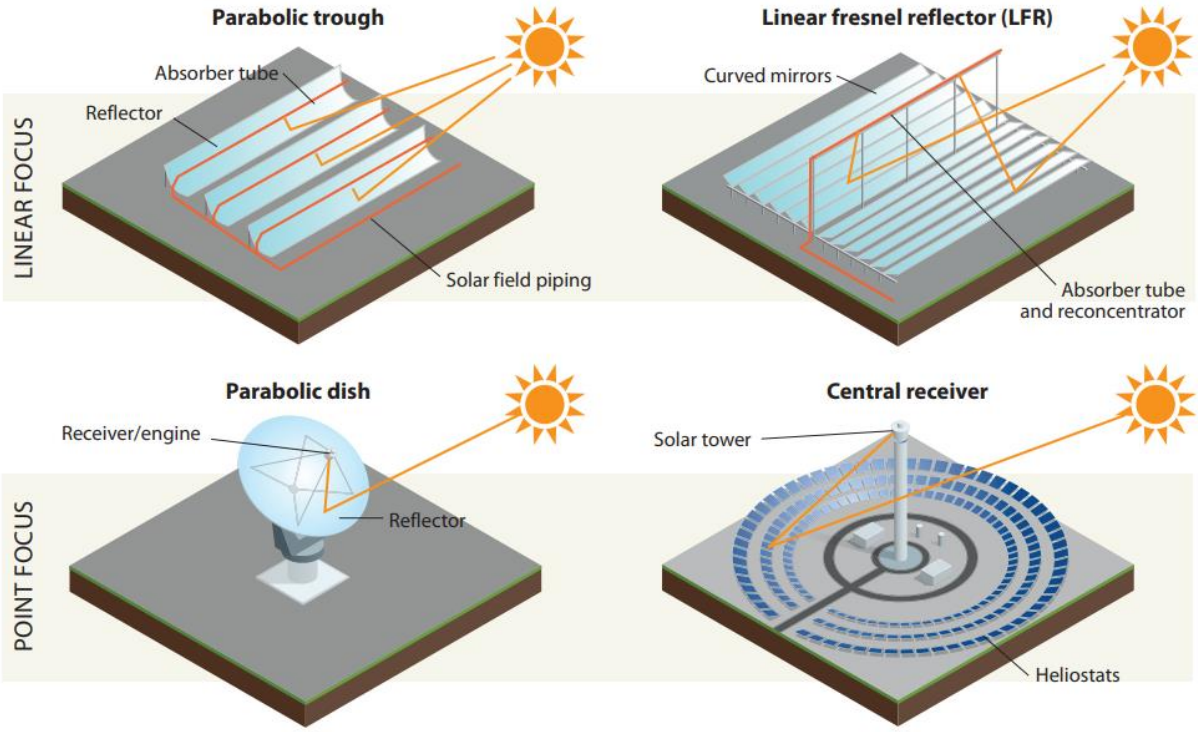

Figure 5 - CSP technologies (World Bank, 2021)

Parabolic trough

This technology allows to concentrate, through parabolic mirrors, the radiation in a tube placed on the focal line. The main components of this technology are the parabolic troughs, the tracking system, the receiver in which the heat transfer medium flows, the storage. In addition, there are the components of a conventional power generation plant, namely the steam generator, the steam turbine, the electric generator and the condenser.

The collectors that reflect the electric radiation, as previously mentioned, have a parabolic shape. The shape of the mirrors is the result of optimization calculations, so that all the existing plants have the same geometric characteristics. In particular, the rim angle (the angle between the optical axis and the line that joins the focal line and the rim) is about 80°, the aperture width 6 m, focal length 1.75 m while the length of a single mirror is about 12-14 m. The mirrors are built in such a way as to allow the reflection of the radiation as much as possible. For this reason, the dominant technology is now made up of “silver coated glass mirrors”. In this case, the reflection occurs through a thin layer of silver that allows a total reflectivity of 93.5%. The bearing structure that supports the mirrors must meet requirements such as high stiffness, lightweight, and should be low cost, since the solar field is the most expensive part of the solar plant.

The receiver is a fundamental component of the plant, since it receives the energy concentrated by the mirrors and transfers it to the thermal storage or steam generator. The receiver consists of a tube in which the heat transfer fluid flows, which is heated in proportion to the dimension of the solar field. Since the distance travelled by the heat transfer fluid can be very high, it is essential that thermal losses are reduced to a minimum. For this reason, the tube coating is made up of several layers that allow for high absorbance in the wavelength range of solar radiation, but at the same time it must ensure low emissivity in the range of thermal radiation (that can be represented by a black body at 400°C). In this way, the heat contained in the heat transfer fluid is dispersed to a lower extent through the walls of the tube. This solution is physically possible through the so-called "selective coating", made up, from the outside towards the inside, of a ceramic layer, a "cermet" layer (ceramic layer with metallic nano-particles) and a metal layer. Typically, to further reduce convective heat losses, there is an additional external glass tube and vacuum is created in the space between the two tubes.

The heat transfer fluid must meet some fundamental requirements. The main objective is to use a fluid that is thermally stable at high temperatures and has a high evaporation temperature. In fact, the higher the temperature of the HTF, the greater the work that can be extracted in the turbine. Furthermore, it is essential to have low freezing temperatures, avoiding as much as possible the need to install backup heaters. Furthermore, the HTF must have a high heat capacity and thermal conductivity, low viscosity, environmentally friendly, low cost and high availability.

The most common HTF(s) are:

- Synthetic thermo oil, which, although reaching low freezing temperatures (12°C), has not very high maximum temperatures, around 400°C. Furthermore, it is relatively expensive and must be replaced periodically.

- Molten salt, which has high freezing temperatures, but at the same time high maximum operating temperatures, around 550 °C. It is available and relatively low cost.

The role of thermal storage is fundamental in CSP plants. In fact, in CSP plants, given a certain electrical power that is to be produced, the size of the solar field is not strictly tied to it and responds to economic optimization criteria. Therefore, an oversized solar field would lead to having to waste a lot of energy, while a solar field that is just big enough to produce the design power implies that the plant produces such power only for a few hours a year. Instead, by installing thermal storage, it is possible to oversize the plant without having to waste part of the energy, since the excess energy produced during the hours with more radiation can be used later when the radiation is absent. In this regard, it is useful to define the "solar multiple" (SM), a parameter that defines how much the solar field is oversized. This parameter is, in fact, the ratio between the maximum thermal power that can

be produced by the solar field and the minimum thermal power necessary to produce the design electrical power. There is a direct proportionality between the SM with the size of the storage and the operating hours of the power block. In this way, thanks to thermal storage it is possible to produce energy on-demand, being able to move production to periods of greater demand, increasing revenues.

Finally, calculating the efficiency of a concentrated solar power plant is a fundamental step in evaluating its performance. The efficiency of a plant, also called "solar-to-electric efficiency", is the ratio between the electrical energy produced and the energy that reaches the panels. This latter quantity is given by the aperture area (i.e., the product of aperture width and trough length) and the direct radiation (G_b) that reaches that surface. This efficiency can also be expressed as the product of the efficiency of the solar field (η_{SF}) and the efficiency of the power block (η_{PB}), according to the formula:

$$\eta = \frac{P_{el}}{A_{ap} G_b} = \eta_{SF} \eta_{PB} \qquad (8)$$

In solar field efficiency, there are optical losses (geometrical inaccuracies, limited optical parameters, shading) and thermal losses due to conduction, convection and radiation. The total efficiency of a system is about 16%.

Figure 6 - Parabolic trough collector in Centro Ricerche Casaccia (ENEA)

Solar tower

Solar tower technology allows to concentrate, through flat or curved mirrors, the radiation in a central point located on a tower. The solar field is composed of mirrors called

"heliostats", which have a two-axis tracking system that allows to orient each mirror independently from the others in the direction of the Sun's rays.

The most common types of heliostats are: canted-glass mirror, that is a single large heliostat divided into sub-mirrors; stretched-membrane heliostat, formed by a mirror with a curved surface; flat or nearly flat mirrors; hexagonal-shaped mirrors. Heliostats can have very different dimensions, from 1 to 150 square meters. The larger the mirrors, the fewer tracking systems and motors are needed, the maintenance costs are reduced but higher investment costs for the foundations are required. In general, the smaller the mirrors, the greater the accuracy in concentrating the radiation.

There are four main types of receivers, i.e. the component placed on the tower that receives the radiation reflected by the mirrors:

- Direct absorption receiver, in which the heat transfer medium is directly exposed to the radiation. A window placed at the top of the tower lets the reflected rays pass through, heating the fluid coming from the upper part of the receiver. Another innovative method involves positioning the receiver at ground level, with the radiation being reflected downwards from the top of the tower.

- External tube receiver, in which vertical tubes are arranged on the external wall of the receiver and are irradiated by the reflected radiation. The flow is pumped from the bottom upwards.

- Cavity receiver, whose operating principle is similar to the Direct absorption receiver, but in this case the fluid, instead of being directly irradiated, flows through coils. This method allows to minimize radiative losses.

- Air receiver, whose main solution is the "open volumetric receiver", in which the radiation is absorbed through modules, placed on the wall of the receiver, formed by a porous material. The radiation, therefore, heats the air present in the porous material.

The efficiency of a solar field is given by the surface-weighted average of the efficiencies of each heliostat. The efficiency of each heliostat is affected by various sources of loss, such as cosine losses (due to the non-perpendicularity of the rays incident on the mirror surface), blocking/shadowing losses (the reflected/incident radiation may be blocked by nearby heliostats), spillage losses (not all the reflected radiation actually reaches the tower), atmospheric attenuation (the radiation may be attenuated by fog, dust etc.).

Linear Fresnel

This technology was developed as an alternative to parabolic trough, with the aim of creating less expensive systems. This technology is based on the principle of Fresnel lenses,

thanks to which, by cutting the surface of a lens creating numerous discontinuous surfaces, the same original result can be obtained, using less material. This principle is also used for mirrors, so that flat mirrors of standardized shape can be built instead of expensive parabolic mirrors. In this way, the greater simplicity of the solar field considerably reduces the investment costs. However, linear Fresnel technology generally produces lower solar-to-electric efficiency values than parabolic trough.

The solar collector system is made up of nearly flat mirrors arranged in parallel rows and a receiver tube positioned at a higher height than the level of the mirrors (generally around 8-11 m). The rows of mirrors cannot be positioned too close to each other, since in these systems the shading and blocking phenomena are particularly accentuated.

The receiver is made up of a tube in which the heat transfer fluid flows and a secondary concentrator. This last component, placed above the absorber tube, is necessary to reflect the rays that do not reach the tube and redirect them towards the tube itself. This component is not present in parabolic trough plants, since in that case it is easier to obtain a precise reflection of the rays. In linear Fresnel plants, it is impossible to produce a precise reflection on the focal line, given the less accurate geometry of the mirrors. Furthermore, the secondary concentrator also allows for better protection from atmospheric agents and better thermal insulation. Another advantage of linear Fresnel plants is that the receiver tube is fixed and does not require flexible connections. In this way, it is possible to use water as a heat transfer fluid, which evaporates directly in the solar field. This solution is not possible for parabolic trough plants, since the high pressures inside the tubes would risk

Figure 7 - Linear Fresnel collector in Centro Ricerche Casaccia (ENEA)

damaging the connections between the tubes. In this way, higher temperatures can be reached and, furthermore, water is an environmentally friendly and economical fluid.

Parabolic dish

This technology allows to concentrate the radiation in a central point through the use of paraboloidal mirrors. This technology, being point-focusing, allows to reach very high efficiencies (up to 30%) and high concentration ratios, resulting in the most efficient technology in the CSP field. However, it is not suitable for large-scale electricity production, since the average power of such plants is in the range from a few kW to a few MW. The energy concentrated in the central point is generally used for the direct production of electricity in Stirling engines, but it can also be transferred to a heat transfer fluid and used in any conventional energy transformation system. The parabolic dish is equipped with a tracking system that allows the dish to always point in the direction of the Sun. The diameter of the dish can vary between 1 and 25 m and the concentration ratios between 1500-4000.

Figure 8 - Parabolic dish collector in Centro Ricerche Casaccia (ENEA)

1.3 Thermal Energy Storage

Energy storage, i.e. the capture of energy at one time for use at a later time, is one of the major energy challenges of the near future. Energy storage is used for various purposes, such as balancing supply and demand, improving the efficiency of systems, reducing the size of plants, and reducing emissions. Among these objectives, balancing supply and demand is the most challenging, as it requires technologies capable of storing large amounts of energy, which must be reliable and accessible at short notice. The development of large-scale storage systems is a very complex challenge because, apart from pumped hydroelectric plants (which are subject to constraints such as environmental and territorial conditions), the technologies enabling large-scale energy storage have not yet reached a sufficient level of maturity and diffusion. The development of this project fits perfectly in this context, since the tank under study will be used to accumulate large quantities of energy coming from large electricity production plants, such as CSP plants.

As mentioned above, the role of large-scale energy storage is fundamental to balance supply and demand. The need to balance supply and demand is mainly due to the ever-increasing and rapid expansion of technologies that exploit renewable energy sources such as solar and wind, which have the disadvantage of being discontinuous and intermittent, depending on atmospheric conditions. As solar and wind installations increase, the ability to efficiently manage peak production will become increasingly important. In fact, the main problem that will arise in the coming years will be an ever-increasing overproduction of electricity (i.e. production is greater than demand) during the central hours of the day. This overproduction of energy can cause instability in the electricity grid, which only works optimally when demand and supply are perfectly balanced. Therefore, in order to avoid curtailment, i.e. the deliberate reduction of electrical energy to a lower level than is actually achievable, energy storage is used to withdraw excess energy during the day and then to release it in the evening, i.e. when renewable energy production is significantly reduced and

demand increases. These considerations are illustrated by the so-called "Duck curve" graph (California Independent System Operator, 2012), which shows the trend of electricity production from dispatchable sources (i.e. energy sources that can be programmed according to demand, such as fossil energy, biomass, hydropower) over the course of a typical day.

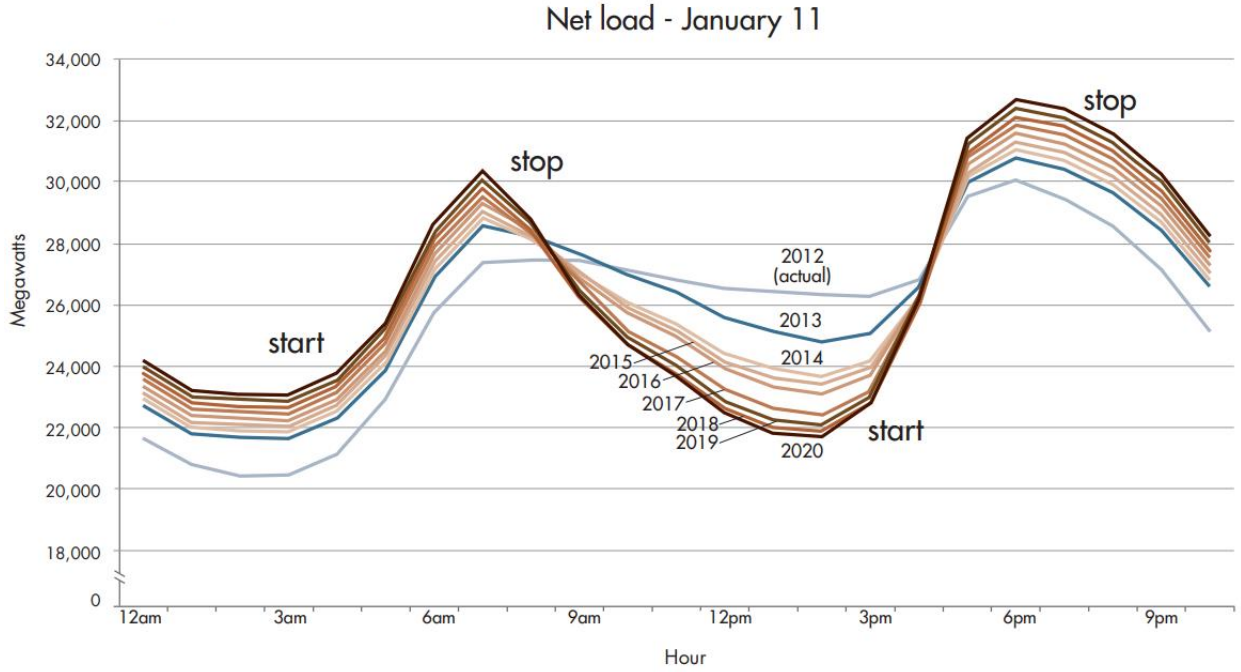

Figure 9 - The "Duck curve" (California Independent System Operator, 2012)

The graph illustrates a notable decline in energy production from dispatchable sources during the central hours of the day, which is offset by an increase in production from renewables. In contrast, energy production remains relatively stable or experiences a slight increase during the evening hours, aligning with the general rise in energy consumption. Consequently, utility companies must significantly and expeditiously increase conventional energy source production during the evening hours. Storage technologies enable the reservation of a portion of the energy required during the evening, thereby ensuring the maximum output from solar systems and reducing the necessity for fossil fuels.

The following figure shows the trend of energy production and consumption in Italy during a typical summer day (in this case, the data refers to 24/07/24 (Terna, 2024)). The graphs show the trend of production from intermittent renewable sources, dispatchable sources and net foreign exchange in a present scenario and in a future one in which energy production from intermittent renewable sources has quadrupled. As it can be seen, in the future scenario there is a huge overproduction, which must be managed through storage systems in order to avoid curtailment.

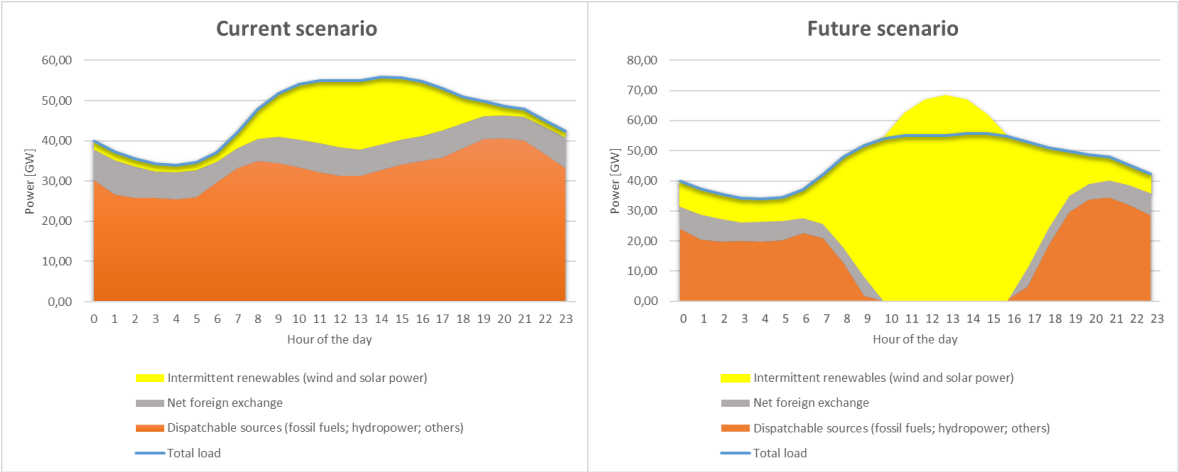

Figure 10 - Trend of power generated on a typical summer day in Italy

1.3.1 Thermal Energy Storage (TES) overview

This paragraph presents an analysis of the fundamental principles of thermal energy storage. TES is one of the main processes that fulfil the essential requirement of storing energy for later use. The process of energy storage comprises three phases, which collectively constitute a cycle: charging, storing and discharging. It should be noted that the aforementioned phases may occur simultaneously and may be repeated several times during a single cycle.

TES can be classified into three principal categories: sensible, latent and thermochemical storages. The selection of an appropriate storage solution is dependent on a number of factors, including economic viability, the required duration of storage, and the quantity of energy that must be stored.

In the case of sensible storage, energy is stored by increasing or decreasing the temperature of the storage medium in comparison to the ambient temperature. In the case of sensible storage, the most utilised medium is water, given its high specific heat value in comparison to other liquids, its extensive availability, low cost and ease of pumping, which facilitates its transportation. In certain instances, however, such as in concentrating solar power (CSP) systems, where reaching high temperatures is necessary, alternative fluids are employed, including molten salt. This kind of thermal storages is preferred for high temperature applications (Kalaiselvam S., 2014).

Latent storages utilise phase changes to store energy. The solid/liquid transformation is usually used and it normally occurs isothermally (Kalaiselvam S., 2014). Latent storages typically employ specific materials known as phase-change materials (PCM), which include various types of hydrated salts and paraffins. The PCM are usually preferred to other

materials since they have high volumetric heat storage capacities and they have wide potential applications (industrial, residential, transport).

Thermochemical storages use the chemical potential of certain substances to store and release energy. In this case, reactive components are necessary and heat storage/release is used to enable the reversible reaction. Usually, an endothermic reaction needs heat in order to dissociate individual components, while heat is released when the components are combined again (exothermic reaction). In thermochemical storages the sorbate (usually a gas/vapor) is trapped into a solid or a liquid material. The sorption processes are called adsorption (in a solid) or absoption (in a liquid). Typical materials involved in these reactions are the salt hydrates (Kalaiselvam S., 2014).

The installation of a TES can result in several benefits, as outlined by (Dincer, 2002), (Kalaiselvam S., 2014):

- Increased generation capacity: surplus production in specific periods can be accumulated for utilisation at a subsequent time, when production is minimal or absent and energy demand is high. Consequently, the overall operational hours of the system are extended, the load factor is increased, and the size of the system can be reduced, since the plant doesn't have to meet the critical load.

- Shift energy purchases: the advantage of shifting the purchase of primary energy is evident in the case of a variable price of energy over time (for example, depending on the period of the day). In this manner, the acquisition of energy can be conducted during periods of lower energy prices, while the storage system provides the requisite energy for the system during other periods.

- Enhance reliability: the incorporation of storage facilitates the enhancement of reliability within a system, as it serves to substitute for the primary energy source in case of malfunction or maintenance.

- Increased energy efficiency: a TES usually produces higher efficiency levels, thanks to the better management of the energy resources. This fact leads also to minimized fossil fuel consumption, lower emissions and higher environmental sustainability.

- Cost reduction: the installation of a TES usually implies reduced overall cost, even though the capital cost is usually higher. In fact, the initial investment for the TES is recovered by the lower operational cost (i.e. fuel purchasing costs).

1.3.2 Molten salt as storage medium

Molten salt (MS) represents the most common means of energy storage in concentrated solar power plants, acquiring a dominant position since the beginning of the development of such plants. Although the use of MS as a storage medium is widely used, its use as a heat

transfer fluid is much less common. Below, a description of molten salt will be proposed, highlighting their main characteristics.

The generic term “molten salt” defines a category of ionic compounds that appear in the solid state under conditions of ambient temperature and pressure, while they are in the liquid state at high temperatures. MS are classified based on the anions of which they are composed, which influence the chemical properties of the mixtures. Molten salt is characterized by a certain temperature range in which they can be used safely, so it is important to define an upper and lower limit of operability. The upper limit is necessary because it identifies the maximum temperature at which the salts are thermally stable and metallic corrosion is kept within certain limits. The lower limit represents the melting temperature of the salts to which a safety range is usually added. Mixtures of salts have lower freezing temperatures than the components taken individually, despite reaching similar stability temperatures. Molten salt is utilized in many industrial applications, thanks to their relatively low-price, high availability, non-toxicity, non-flammability, high thermal capacity, high viscosity, high density, high thermal stability, low vapor pressures (Bauer, 2021), (Lantelme, 2013).

When, in the context of CSP systems, we talk about molten salt, we are generally referring to a specific type of salt, the so-called *Solar salt*. Solar salt is a non-eutectic mixture of molten salt composed of 60% sodium nitrate ($NaNO_3$) and 40% potassium nitrate (KNO_3). These types of salts are commonly used as fertilizers, making them cost-effective and easily available. Solar salt has a freezing temperature of approximately 260°C, but is generally used at temperatures above 290°C for safety reasons. The maximum temperature at which it is considered thermally stable is approximately 560°C. The main limitation of Solar Salt concerns the possible freezing of the salts during the operational phases. This condition must be avoided both if it is used as a storage medium and as an HTF. For this reason, it is often necessary to install backup heaters which intervene if the temperature drops below a certain threshold (typically during the night). When using MS, corrosion risks must also be carefully monitored.

The cost of molten salt is approx 4-20 $€/kWh_{th}$ (considering a temperature difference of 250 K), constituting an important fraction of the total cost of the TES (Bauer, 2021).

1.3.3 Molten salt storage configurations

There are three main thermal storage configurations for CSP systems:

- Two-tank indirect configuration.
- Two-tank direct configuration.
- Single-tank configuration.

The first two solutions are mature technologies and widely used in existing plants, while the last configuration is still being studied and is not yet considered a mature technology.

Precisely this last solution is the subject of study in this paper, since it is based on the principle of thermocline thermal storage.

The state of the art of storage tanks for CSP systems is represented by unpressurized tanks with flat bottoms. Each tank has a maximum height of 13 m and a maximum diameter of 40 m, dimensions that allow the storage of approximately 30,000 tonnes of salts (Bauer, 2021). Each tank is equipped with foundations and thermal insulation. Thermal storages for CSP systems have different storage capacities, in a range that varies around 3-15 hours (on average, 7 hours). It should be remembered that to define the capacity of a thermal storage it is generally expressed as the quantity of hours in which the storage can provide the nominal thermal power to the system.

Below, the configurations considered are explained in detail:

- Two-tank configurations: in these configurations there are two tanks, one contains the cold fluid (which will be heated by the solar concentration system) and one the hot fluid (which is stored and then used to produce electricity). This solution allows, thanks to the variation of the volume in each tank, to maintain a constant temperature in each tank during all phases of operation of the system, which makes the power production system more efficient, being able to operate in constant conditions and always producing the nominal power. This type of configuration allows the heat exchangers to be sized only on the basis of the expected nominal electrical power and not on the basis of the storage capacity. Therefore, an increase in storage capacity does not imply any modification to the power production system. This aspect makes the additional investment costs very low if you want to increase storage capacity.

  The previous considerations are valid for both two-tank configurations. What, however, distinguishes these two configurations is the choice of heat transfer fluid. In fact, in the *Two-tank indirect configuration*, the HTF is different from the storage medium. In fact, the HTF flows in a loop physically separated from the fluid present in the storage. It takes heat from the solar field and transfers it through heat exchangers to the storage. Instead, in the case of *Two-tank direct configuration*, the fluid that transfers heat from the solar field to the storage is the same. This last solution allows to avoid the installation of heat exchangers inside the storage, thus being more economical. However, it is not always possible to apply this configuration. In fact, if the solar system uses parabolic trough technology, the use of a direct configuration would make the risk of freezing of MS along the long pipes in solar field very high. For this reason, for this type of system, an indirect configuration is almost always used, being able to use fluids with lower freezing temperatures, such as synthetic oils, as HTF.

In contrast, the direct configuration is often used for systems based on solar tower technology. In these cases, in fact, the pipes are generally shorter and easier to insulate or heat if the temperature is too low. Therefore, it is possible to circulate the molten salt directly in the solar tower, so the heat transfer fluid and the storage fluid coincide (Bauer, 2021). Below, a schematic representation of the two plants is shown, taken from (Lantelme, 2013):

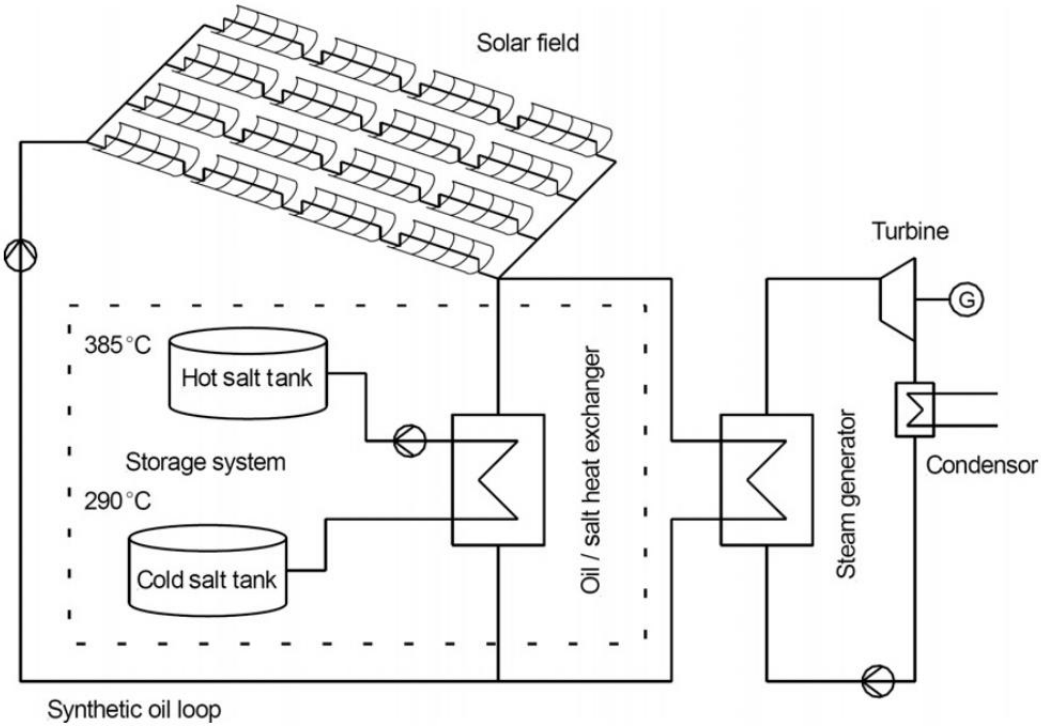

Figure 11 - Two-tank indirect configuration (Lantelme, 2013)

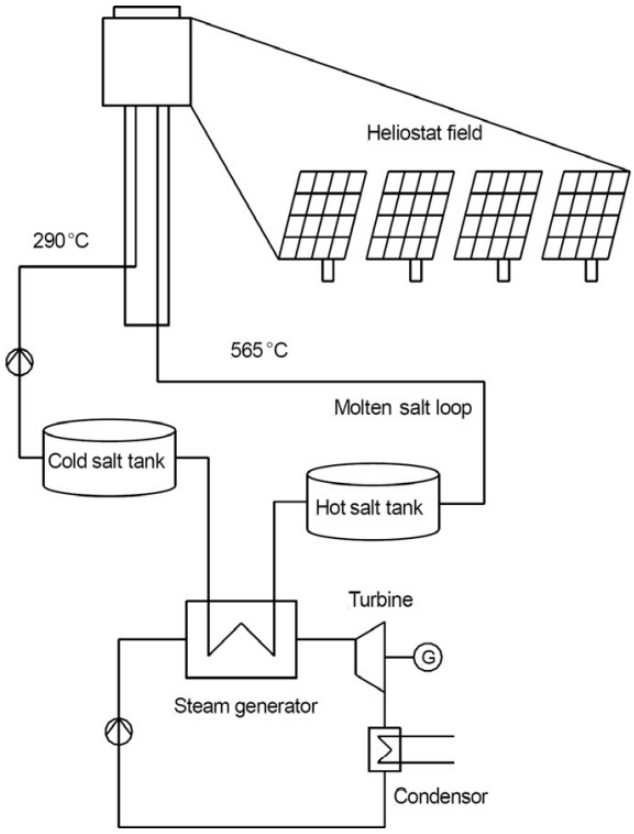

Figure 12 - Two-tank direct configuration (Lantelme, 2013)

- Single-tank configuration: this configuration involves the installation of a single thermal storage which provides the system with both cold and hot fluid. This solution is possible thanks to the stratification specifically created inside the tank, in which the upper area is at a higher temperature than the lower area. The stratification is due to the buoyancy force, which allows the fluid with a higher temperature to rise towards the upper part of the tank by virtue of its lower density. On the contrary, in the lower zone the fluid has a lower temperature and a higher density. The transition zone between the warm zone and the cold zone is called the *thermocline*. The smaller the thickness of the thermocline zone, the greater the stratification and the greater the efficiency of the TES. In particular, the exergy study of a stratified tank will be described below, in which it is noted that a stratified TES has a greater exergy than the same completely mixed tank. The choice to install this type of configuration compared to configurations with two tanks is mainly due to economic reasons, given that a configuration with a single tank can lead to a reduction of 1/3 in investment costs (Pacheco, 2002). This saving in economic terms, however, implies a lower total efficiency of the system, given that the temperatures of the cold and hot fluid do not remain constant. Indeed, in this configuration, the temperature of the hot fluid decreases during the discharge, which influences the operation of the power block and the electrical energy generated. This aspect is due to the mixing between hot and cold fluid inside the tank, which causes a destruction of exergy (Cagnoli, 2023). In the following figure, taken from (Ratnu S. S., 2021), the schematic representation of a CSP plant with a thermocline storage is shown:

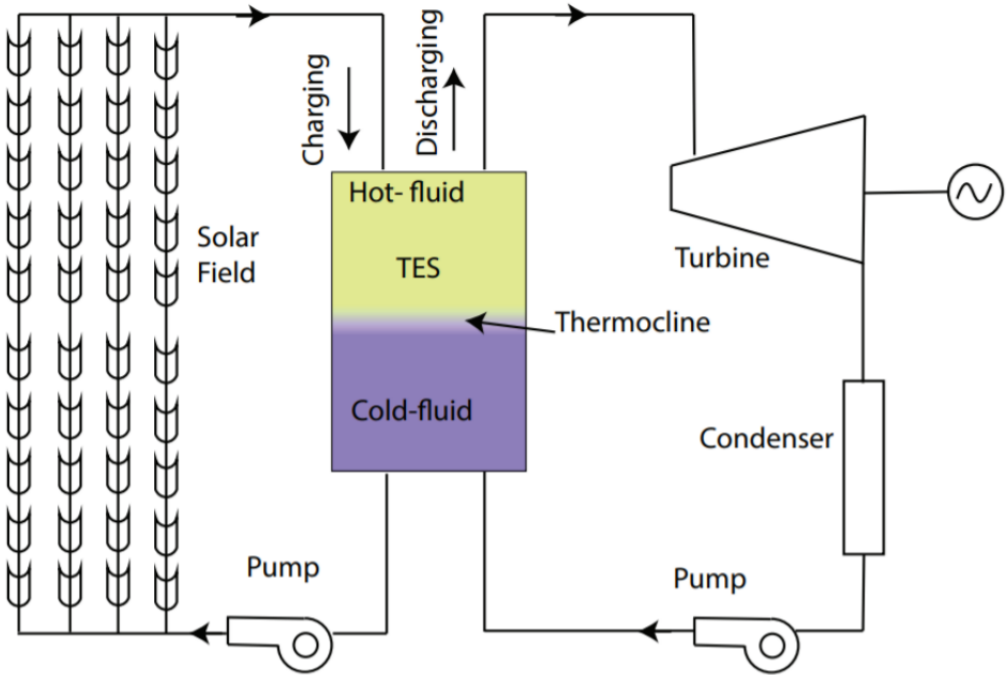

Figure 13 - Single-tank configuration (Ratnu S. S., 2021)

1.3.4 Energy and exergy analysis of an indirect TES

In this section, it was decided to carry out an energetic and exergetic analysis according to the methodology described by (Dincer, 2002). An energetic analysis is based on the fundamental principle of the first law of thermodynamics, namely the conservation of energy. This type of analysis involves the study of the flows entering and leaving a thermodynamic system, thereby facilitating the acquisition of significant insight into the losses and efficiency of the system. However, this type of analysis does not provide an accurate assessment of the actual level of system performance relative to the ideal. It is therefore necessary to conduct an exergy analysis in order to gain a deeper understanding of the system and identify the areas where efficiency is compromised, as well as the underlying causes. Exergy is defined as the maximum quantity of useful work that can be extracted, through ideal and reversible transformations, in order to bring a system to equilibrium with the surrounding environment. Consequently, an exergy analysis enables the quality of a specific energy source and the extent of its degradation during a process to be evaluated. In general, the exergy of a given source or flow of energy is directly proportional to the extent of its deviation from the thermodynamic properties of the external environment.

In general, two broad categories of systems can be considered: direct (open) and indirect (closed). In direct systems, mass, heat and work can be exchanged across the surface and volume of the system. In contrast, in indirect systems, only heat and work can be exchanged. As the thermal storage system developed in this thesis is a indirect system, it was decided that a thermodynamic analysis should be carried out for this category of systems.

The case considered, illustrated in the following figure, consists of a thermal storage that undergoes the charging, storing and discharging phases.

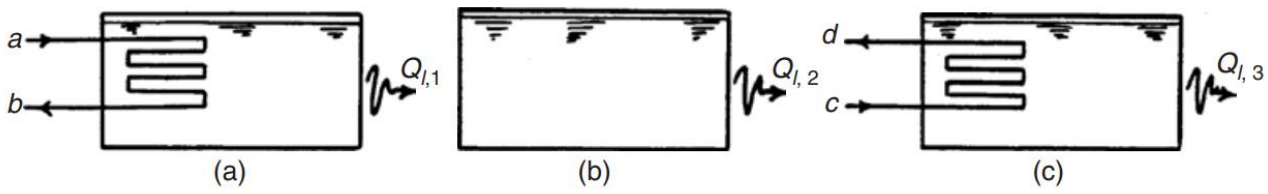

Figure 14 - Charging (a), storing (b) and discharging (c) phases (Dincer, 2002)

The system has the following characteristics:

- The external walls of the system are not adiabatic.
- The walls of the coil tubes are considered adiabatic.

- The external environment is in fixed conditions of temperature and pressure.
- The storage volume is constant.
- The work carried out externally on the system is considered negligible.
- The potential and kinetic energy components are considered negligible.
- Charge and discharge flows are considered stationary and one-dimensional.

From the energy balance, the stored energy is given by the difference of the energy introduced into the system (charge) and the sum of the energy removed (discharge) and the thermal losses, according to the formula:

$$(H_a - H_b) - [(H_d - H_c) + Q_{loss}] = \Delta E \quad (9)$$

Where H_k is the total enthalpy of the state $k = a, b, c, d$; Q_{loss} is the sum of all the heat losses during the process; ΔE is the accumulation energy. These last two items can be expressed as:

$$Q_{loss} = Q_{loss,charging} + Q_{loss,storing} + Q_{loss,discharging} \quad (10)$$

$$\Delta E = E_f - E_i \quad (11)$$

Where E_i and E_f are the initial and final total energy in the storage.

From the exergy analysis point of view, similar considerations can be carried out, as shown in the following equations:

$$(\in_a - \in_b) - [(\in_d - \in_c) + X_{loss}] - I = \Delta\Xi \quad (12)$$

$$I = I_{charging} + I_{storing} + I_{discharging} \quad (13)$$

$$X_{loss} = X_{loss,charging} + X_{loss,storing} + X_{loss,discharging} \quad (14)$$

$$\Delta\Xi = \Xi_f - \Xi_i \quad (15)$$

Where $\in_k$ are the total exergies of the flows $k = a, b, c, d$; X_{loss} is the exergy loss that corresponds to Q_{loss}; I is the exergy destruction (also known as *irreversibility*); $\Delta\Xi$ is the exergy accumulation; Ξ_i and Ξ_f are the initial and final exergy contents of the system.

The following expression of $\in_k$ and $X_{loss,j}$ can be evaluated, considering j one of three phases:

$$\in_k = (H_k - H_0) - T_0(S_k - S_0) \quad (16)$$

$$X_{loss,j} = \left(1 - \frac{T_o}{T_j}\right) Q_{loss,j} \tag{17}$$

Where H_0 and S_0 are the total enthalpy and total entropy at the environment conditions. These expression can be derived neglecting chemical exergy (since for sensible TES it does not have any contribution to the exergy flows), potential and kinetic exergy components. Furthermore, the tank is considered fully mixed and the temperatures T_j are constant during each phase *j* (usually T_j is considered as the tank mean temperature).

Considering a complete cycle, in which the initial and the final states are equal, the following efficiencies for energy and exergy can be defined:

$$\eta = \frac{Discharging\ energy}{Charging\ energy} = \frac{H_d - H_c}{H_a - H_b} = 1 - \frac{Q_{loss}}{H_a - H_b} \tag{18}$$

$$\psi = \frac{Discharging\ exergy}{Charging\ exergy} = \frac{\epsilon_d - \epsilon_c}{\epsilon_a - \epsilon_b} = 1 - \frac{X_{loss} + I}{\epsilon_a - \epsilon_b} \tag{19}$$

Some similar considerations can be carried out for each cycle phase instead of studying the whole cycle. In the following, as an example, the charging phase analysis is presented. The storing and discharging equations can be found in a similar way.

The energy balance equation and efficiency are presented below:

$$(H_a - H_b) - Q_{loss,charging} = \Delta E_{charging} \tag{20}$$

$$\Delta E_{charging} = E_{f,charging} - E_{i,charging} \tag{21}$$

$$\eta_{charging} = \frac{Energy\ accumulation}{Energy\ input} = \frac{\Delta E_{charging}}{H_a - H_b} \tag{22}$$

While, in the following, the exergy balance equation and efficiency are shown:

$$(\in_a - \in_b) - X_{loss,charging} - I_{charging} = \Delta \Xi_{\text{charging}} \tag{23}$$

$$\Delta \Xi_{\text{charging}} = \Xi_{\text{f,charging}} - \Xi_{\text{i,charging}} \tag{24}$$

$$\psi = \frac{Exergy\ accumulation}{Exergy\ input} = \frac{\Delta \Xi_{\text{charging}}}{\epsilon_a - \epsilon_b} \quad (25)$$

Finally, it can be verified that the overall energy and exergy efficiencies can be calculated as the product of charging, storing and discharging efficiencies.

1.3.5 Exergy analysis of a thermally stratified TES

In this part of the thesis, it was decided to carry out an exergy analysis of thermal stratified storage. This decision is based on the fact that thermocline storage, which is developed and studied in this paper, falls within the category of thermally stratified storage, as its primary objective is to divide the tank into two distinct zones with varying temperatures.

The study of exergy is particularly important in the context of this type of heat accumulation. Indeed, if we consider two thermal storages, one not thermally stratified and the other thermally stratified, which have the same amount of energy, we observe that they have different amounts of exergy. This is because the energy analysis does not take into account the quality of the energy. In general, when two flows at different temperatures are combined, even if thermal losses are negligible, a loss of exergy in the system still occurs. Consequently, the resulting stream has a reduced qualitative value compared to the two separate streams. It is therefore crucial to optimise the management of the charging, storing and discharging phases in thermocline storage in order to achieve the strongest possible separation between the hot and cold areas, thereby maximising the exergy of the system. The effectiveness of a thermocline storage system is therefore inversely proportional to the thickness of the separation zone between the hot and cold zones. The separation zone is defined with the term *thermocline*.

The calculation of energy and exergy quantities for thermally stratified storages can be performed using either numerical or analytical methods. In this section, the methods belonging to the second category are proposed, with reference to the models developed by (Dincer, 2002). Analytical models offer an excellent balance between accuracy and practicality, providing a sufficiently realistic, simple and flexible representation of complex phenomena. In all models the temperature is assumed to depend only on the height of the tank (considered in a vertical position), therefore the temperature distribution is one-dimensional.

The energy and exergy in a TES can be evaluated integrating their specific values over the mass:

$$E = \int e \, dm \tag{26}$$

$$\Xi = \int \zeta \, dm \tag{27}$$

Where e and ζ are the specific energy and exergy. These quantities, for ideal liquid having constant specific heat and environment temperature equal to T_0, can be found thanks to the equations *(28)* and *(29)*:

$$e(T) = c(T - T_0) \tag{28}$$

$$\zeta(T) = c(T - T_0) - c\, T_0 \ln\left(\frac{T}{T_0}\right) = e(T) - c\, T_0 \ln\left(\frac{T}{T_0}\right) \tag{29}$$

Considering a mono-dimensional temperature distribution along the tank vertical direction *h,* the horizontal mass element can be defined as:

$$dm = \frac{m}{H} \, dh \tag{30}$$

Where H is the tank height. Since the temperature depends only on the height, also the specific energy and exergy depend only on height. Consequently, the following relations can be found:

$$E = \frac{m}{H} \int_0^H e(h) \, dh \tag{31}$$

$$\Xi = \frac{m}{H} \int_0^H \zeta(h) \, dh \tag{32}$$

Considering that the mean temperature of the tank in case it is fully mixed can be defined as:

$$T_m = \frac{1}{H} \int_0^H T(h) \, dh \tag{33}$$

The total energy can be calculated through the following equation:

$$E = mc\ (T_m - T_0) \tag{34}$$

In a similar way, the exergy of the stratified TES in expressed in the *(35)*:

$$\Xi = E - mcT_0 \ln\left(\frac{T_e}{T_0}\right) \tag{35}$$

Where T_e is the equivalent temperature of a mixed TES with the same total exergy as the stratified one. T_e depends on the degree of stratification. The expression that defines this quantity is:

$$T_e = \exp\left(\frac{1}{H}\int_0^H lnT(h)\ dh\right) \tag{36}$$

Finally, from *(35)*, the exergy of a fully mixed TES is equal to:

$$\Xi_{\mathrm{m}} = E - mcT_0 \ln\left(\frac{T_m}{T_0}\right) \tag{37}$$

The difference between the exergy of the stratified TES and the mixed TES is equal to the minimum work necessary to create the stratification and is given by the following equation:

$$\Xi - \Xi_m = mcT_0 \ln\left(\frac{T_m}{T_e}\right) \tag{38}$$

In the following, three different methods to define the temperature distribution are exposed: linear, stepped and continuous-linear. The input data is the temperature distribution, while the outputs are T_m and T_e, fundamental parameters to calculate energy and exergy in the stratified TES.

- Linear profile: the distribution of the temperature is linear. The bottom temperature is defined as T_b *(h=0)* and the top temperature T_t *(h=H).* The temperature distribution, the mean temperature and the equivalent temperature can be derived:

$$T(h) = \frac{T_t - T_b}{H}\ h + T_b \tag{39}$$

$$T_m = \frac{T_t + T_b}{2} \tag{40}$$

$$T_e = \exp\left[\frac{T_t\,(lnT_t - 1) - T_b(lnT_b - 1)}{T_t - T_b}\right] \tag{41}$$

- Stepped profile: in this case, the volume is divided into k horizontal zones, each one described by a constant temperature. In order to carry out the next calculations, it is necessary to define the mass fraction of each zone:

$$x_j = \frac{m_j}{m} \tag{42}$$

Where m is the total mass and the mass of each zone m_j is equal to:

$$m_j = \rho A(h_j - h_{j-1}) \tag{43}$$

Where h_{jC} and h_{j-1} are the top and bottom heights of each zone j. If the cross section A is constant, the mass fraction is equal to:

$$x_j = \frac{h_j - h_{j-1}}{H} \tag{44}$$

Consequently, it can be found that the mean and equivalent temperatures can be expressed as:

$$T_m = \sum_{j=1}^{k} x_j T_j \tag{45}$$

$$T_e = \exp\left(\sum_{j=1}^{k} x_j\, lnT_j\right) \tag{46}$$

- Continuous-linear profile: the temperature distribution is composed of k horizontal zones. In each zone the temperature varies linearly from the bottom to the top, following the equation for each j zone:

$$\phi_j(h) = \frac{T_j - T_{j-1}}{h_j - h_{j-1}}\, h + \frac{h_j T_{j-1} - h_{j-1} T_j}{h_j - h_{j-1}} \tag{47}$$

The mean and equivalent temperature can be found through the following equations:

$$T_m = \sum_{j=1}^{k} x_j \frac{T_j + T_{j-1}}{2} \tag{48}$$

$$T_e = \exp\left(\sum_{j=1}^{k} x_j \ln(T_e)_j\right) \tag{49}$$

Where $(T_e)_j$ is equal to:

$$(T_e)_j = \begin{cases} \exp\left[\dfrac{T_j(lnT_j - 1) - T_{j-1}(lnT_{j-1} - 1)}{T_j - T_{j-1}}\right], & if\ T_j \neq T_{j-1} \\ T_j, & if\ T_j = T_{j-1} \end{cases} \tag{50}$$

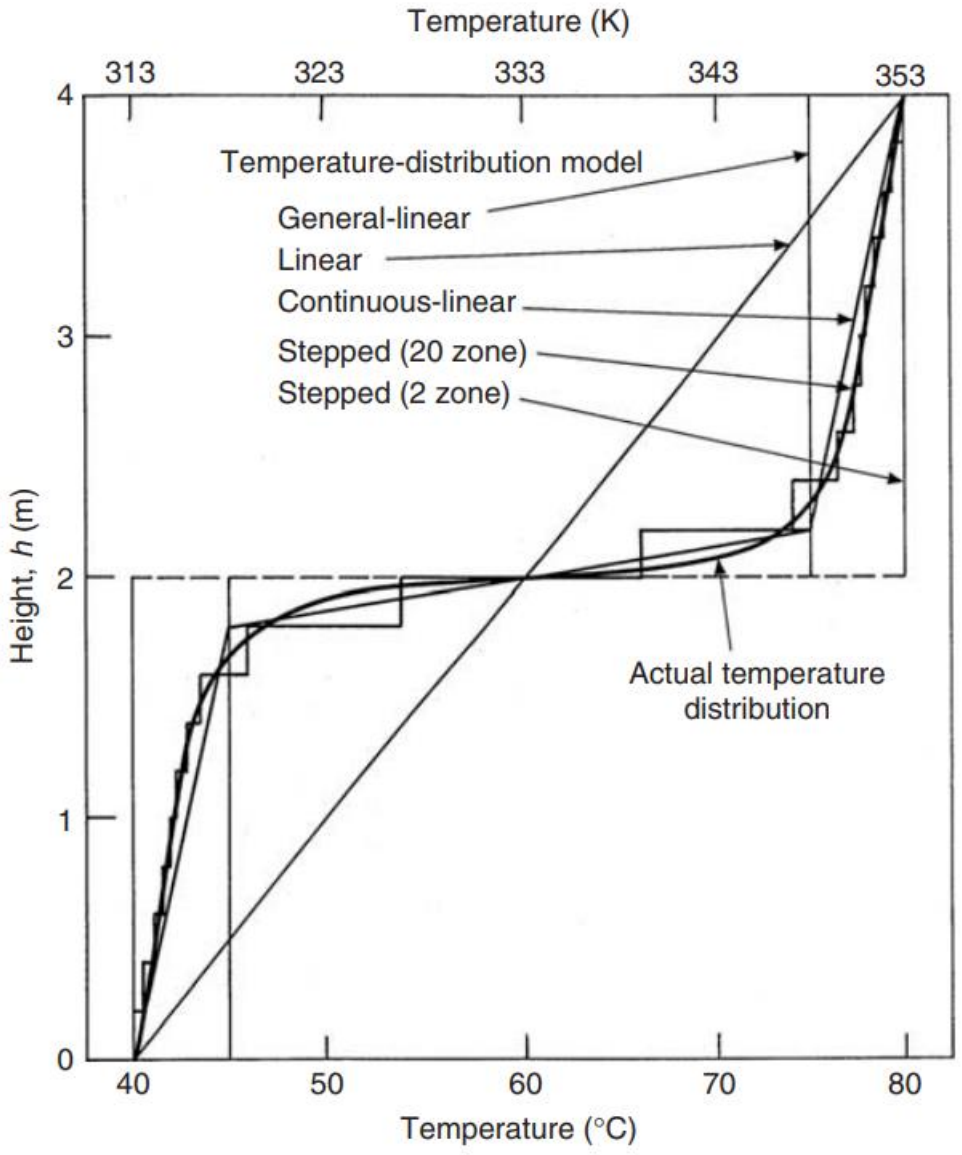

Figure 15 - Methods to define the temperature profiles in a thermocline TES (Dincer, 2002)

In general, the three methods achieve different levels of accuracy. The linear method is not very flexible and generally not very accurate, although it can be useful if the thermocline area is particularly large. The stepped profile and continuous linear can reach very high levels of accuracy as the number of nodes increases. In general, the stepped profile requires slightly less computational complexity than the continuous linear, so it becomes preferable if the number of nodes is particularly high. On the contrary, the continuous linear method is sufficiently accurate even with a small number of nodes, as in the well-known case of the three-zone temperature distribution, in which there are only 3 zones (hot, cold and thermocline).

To objectively evaluate the level of stratification present in different TES, it is useful to calculate the ratio between the exergy of the stratified storage and that of the mixed one. This ratio, independent of mass and specific heat, is always greater than 1. The higher the value of the ratio, the higher the level of stratification inside the tank. The expression that defines this quantity is shown below:

$$\frac{\Xi}{\Xi_m} = \frac{\frac{T_m}{T_0} - 1 - \ln\left(\frac{T_e}{T_0}\right)}{\frac{T_m}{T_0} - 1 - \ln\left(\frac{T_m}{T_0}\right)} \qquad (51)$$

The ratio, considering a constant average temperature, is inversely proportional to the thickness of the thermocline area and, in general, the more significant the temperature changes within the bearing, the more the ratio increases. However, by varying the average temperature, the ratio decreases with increasing temperature, as high temperatures produce more exergy, so the stratification effect is less relevant.

1.4 Microwave heating

Microwaves (MW) are electromagnetic radiations with wavelengths shorter than radio waves and longer than infrared radiation. The frequency range of microwaves is generally considered to be between 0.3 and 300 GHz. Microwaves, although their best known use is for domestic use with microwave ovens, are commonly used for heating in numerous industrial processes, such as waste treatment, vitrification, synthesis of inorganic compounds, etc. However, in recent years the study of microwaves has also begun to be directed to the energy sector, being a valid tool for discharging energy into thermal storage. In fact, microwaves allow electrical energy to be transformed directly into heat.

Microwave heating, by transforming electrical energy into heat, is considered a valid alternative to heating by the Joule effect, carried out using electrical resistances. In this sense, MW heating has some advantages over the Joule effect (Rodríguez-García M. M., 2023):

- MW heating is a volumetric process. This aspect allows the fluid to be heated more homogeneously, avoiding excessively high temperature peaks on the walls. In fact, in the case of Joule heating, wall heating implies that the highest temperature of the salts is on the surface, with the risk of high local temperature peaks with damage to the salts.

- MW heating has a very rapid response in switching off and on. This aspect allows for the use of high heating rates and energy savings.

- Joule heating is not particularly effective if the fluid to be heated has a low heat conductivity, such as, for example, molten salt.

The heating mechanism of a material through MW and the calculation of the dissipated power is described below. When microwave radiation strikes a dielectric material (i.e. one that has polar ions or molecules), the dipoles present in the material tend to oscillate and align themselves in the direction of the electric field of the waves. As the molecules move to align themselves with the

field (a phenomenon called "dipolar polarisation"), thermal energy is dissipated by friction, causing the temperature of the irradiated material to rise.

Before describing the energy dissipation equation, it is necessary to introduce some specific quantities of dielectric materials, namely the dielectric properties. The electrical permittivity (ε) of a material measures the polarizability of a dielectric material. The higher the permittivity, the greater the ability of the particles to align themselves with the electric field. The electrical permittivity is given by the product of the permittivity in free space (ε_0) and the relative permittivity of the material (ε_r). The permittivity is a complex quantity that is formed that the real part (dielectric constant) and the imaginary factor (loss factor), as shown in the formula below:

$$\varepsilon = \varepsilon_0 \varepsilon_r = \varepsilon' + i\varepsilon'' \quad (52)$$

The dielectric constant measures how much energy from the electric field can be stored in the material, while the loss factor measures the dissipation of the energy in the material. If the loss factor is enough high ($\varepsilon'' > 0.1$) the material can be heated by microwaves, while if it's low ($\varepsilon'' < 10^{-3}$) the material is transparent to MW radiations. The loss tangent, $\delta = \tan\left(\frac{\varepsilon''}{\varepsilon'}\right)$, quantifies the conversion efficiency of electromagnetic energy into heat.

The fundamental equation that describes the power absorbed in the material, considering an homogeneous electric field (ε'') established in the MW expansion volume is shown in the following formula:

$$P = 2\pi f E^2 \, \varepsilon_0 \varepsilon_r \tan(\delta) \quad (53)$$

Where f is the microwave frequency.

Another quantity that is usually used to describe the capacity of a material to absorb MW energy is the penetration depth, i.e. the distance from the surface at which the electric field is attenuated to 1/e:

$$D_p = \frac{\lambda_0 \sqrt{\varepsilon'}}{2\pi\varepsilon''} = \frac{\lambda_0}{2\pi\sqrt{\varepsilon'}\tan(\delta)} \quad (54)$$

Where λ_0 is the wavelength of the MW radiation.

The most used microwave radiation frequencies in the industrial field are 0.915 GHz and 2.45 GHz. In fact, these frequencies are particularly suitable because they do not interact with the frequencies used for communication, being used in the scientific/medical/industrial field. Furthermore, low frequencies are more suitable for heating, increasing the penetration depth (Joseph, 2017).

The main components of a MW heating system are the magnetron (microwave generator), the waveguide (aluminum tubes to guide the radiation to the applicator) and the applicator. The applicator can have different shapes and is usually made of a metal chamber (batch operation) or a tunnel with a conveyor belt (continuous operation) (Joseph, 2017). Often, a stirrer (rotating fan) is present, uniforming the heating in the material. It is useful to specify that all metal components reflect microwave radiation.

1.5 Aim of the thesis

After having carried out the necessary theoretical considerations, the next section is dedicated to the experimental study carried out through numerical simulations on the CFD software STAR-CCM+. It is therefore necessary to briefly clarify the objectives that this thesis intends to achieve.

In this thesis, it was decided to bring some developments and innovative elements to a thermocline thermal storage developed by ENEA. ENEA has, in fact, developed a prototype of a storage tank equipped with heat exchangers inserted in a channel arranged vertically in the centre of the tank. The heat exchangers are used for the charging and discharging phases, while the central channel is used to increase the temperature stratification in the tank.

The main objective of this work is to insert a device that allows the tank to be charged thanks to microwaves and to study charging phase from a fluid dynamic point of view. The fluid dynamic study is carried out with CFD simulations. Furthermore, this thesis aims to improve the performance of the thermocline storage (i.e. increase the temperature stratification) by modifying the geometric characteristics of the channel.

In the following, after showing the characteristics of the developed models, the results and conclusions deriving from the simulations are presented.

PART 2

This macro part of the thesis is dedicated to the description of the models developed and the results obtained. First, the concept of thermocline storage conceived by ENEA is described. This concept is the basis of all the models studied in this thesis. Then, the main characteristics of the CFD models developed are described. Finally, the results of the simulations carried out are presented.

2.1 ENEA thermocline storage

The basic concept on which the models developed in this work are based is a thermocline energy storage system designed by ENEA. The thermal storage system developed and tested by ENEA was designed within the ORC-PLUS project (Organic Rankine Cycle – Prototype Link to Unit Storage) (Russo V., 2018) in order to install a 20 MWh storage in a CSP solar plant with linear Fresnel technology located in Ben Guerir in Morocco. ENEA has developed a prototype of the storage tank with a total capacity of 200 kWh in the Casaccia Research Center (Rome, Italy). The following image shows the main features and components:

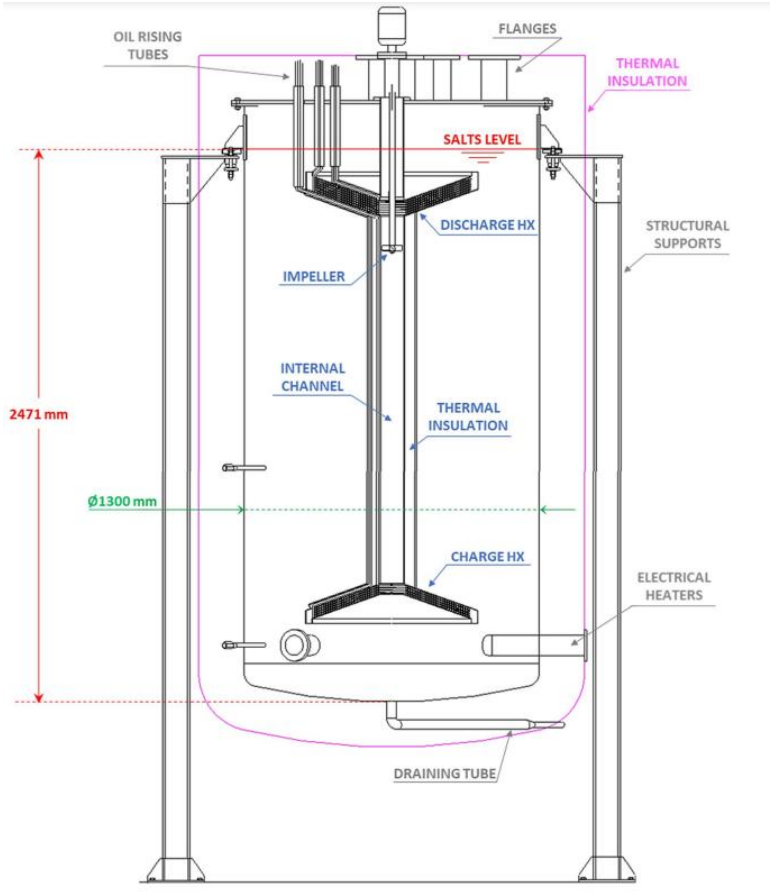

Figure 16 - Thermocline TES developed by ENEA (Zanino R., 2020)

The system is equipped with the following components (Gaggioli W., 2020):

- Storage tank: the storage tank consists of a cylindrical body with a radius of 1.3 m and a height of 2.471 m. The cylindrical body is closed in the lower part by a shell that allows it to counteract the hydrostatic pressure of the salts, while in the upper part there is a horizontal plate in which there are some flanges necessary for measurements and other operations. One of these allows the maintenance of atmospheric pressure inside the tank.

- Internal channel: this component is the fulcrum of the entire tank and constitutes its main innovation compared to conventional tanks. It consists of a channel positioned on the tank axis and the external diameter measures 101.6 mm (4''). In the lower and upper part, the channel widens acquiring a conical shape in order to accommodate the heat exchangers.

- Charge heat exchangers: it consists of 4 coils that form a conical-shaped bundle. Each coil completes 28 loops. The heat exchanger is located in the lower part of the tank and is inside the central channel.

- Discharge heat exchangers: it is made up of 6 coils of 28 loops that form a conical bundle in the upper part of the channel.

- 3 electrical heaters: two of these are necessary to compensate for heat losses during the non-use phase of the system and to maintain the correct temperature before starting the test phases; an additional heater is provided to simulate the charging phase, performing the same task normally performed by the CSP system.

- Pump: located outside the tank, it is necessary to circulate the diathermic oil inside the heat exchangers.

- Air cooler: it is used to cool the heat transfer fluid during the discharge phase, simulating an Organic Rankine Cycle (ORC).

- Expansion vessel: to monitor and manage the volume variations of the heat transfer fluid.

- Valves: there are two three-way valves to manage the charging and discharging phases; some vent valves to maintain the internal pressure within adequate limits; a safety valve in case high pressures are reached inside the tank.

- Impeller: it is positioned in the upper part of the internal channel and aims to regulate the mass flow rate in order to enhance the temperature stratification inside the tank.

The operational functioning of the tank is explained in the following. In the charging phase, the heat transfer fluid (diathermic oil in this case), passes through the solar field, storing and transporting the heat coming from the solar radiation concentrated in the receiver tube (inside which the fluid flows). Subsequently, the HTF, which is at a high temperature, flows inside the charging coil, releasing heat to the molten salt. In the tank, MS, acquiring heat, increase in temperature and decrease in density. In this way, thanks to the effect of natural convection, the hot molten salt rises along the channel and stratify in the upper part of the tank. It should be noted that the hot fluid during the rise along the internal channel does not influence the temperature stratification in the tank, since the channel is insulated. In the meantime, the diathermic oil, having released heat to the molten salt, exits the coil at a lower temperature and is re-introduced into the solar field to continue the cycle.

During the discharge phase, on the other hand, the heat transfer fluid, in the upper part of the tank, flows along the discharge coil acquiring heat from the salts (which are at a high temperature) and increasing its temperature. Subsequently, the heat acquired by the salts is used in the ORC cycle to produce electrical energy. The molten salt, giving off heat to the HTF, is cooled, thus increasing their density. In this way, having acquired a higher density than the fluid below, they descend along the channel, arranging themselves in the lower part of the tank.

2.2 Hybridized Thermocline TES

The models developed in this thesis were created using as a starting point the thermal storage developed by ENEA, to which some modifications were applied. In particular, the most innovative element is represented by the device that allows the storage to be charged through microwaves (MW). MW represent an innovative and promising method to transform electrical energy into heat, which is attracting increasing interest in research in the energy sector.

The main reason why it was decided to develop a prototype that allows microwave heating is the possible hybridization between CSP technologies and photovoltaics. In fact, as seen in the *Introduction*, a very high growth of photovoltaic plant installations is expected in the coming years, with the consequent need to store the energy exceeding the demand during the hours in which solar radiation reaches its daily peak. CSP plants, since they are always equipped with thermal storages, represent an ideal solution to collect the excess energy from PV plants. This solution ensures a reduction in investment costs, greater grid stability and greater efficiency of the plants involved. MW, thus, represent an efficient and innovative method to transform the electrical energy of PV systems into heat and charge the thermal storage of CSP systems.

In order to carry out this hybridization between the two technologies, *Hybridized Thermocline TES* models have been developed, which can be charged both with the thermal energy of CSP systems and with the electrical energy of PV systems (through microwaves). The device with which the MW are introduced into the tank consists of two waveguides and a microwave expansion volume equipped with a ceramic window. The waveguides guide the microwaves (generated outside the tank) into the lower part of the tank. The expansion volume, filled with air, is necessary to expand the MW and make the electric field more homogeneous, resulting in more uniform volumetric heating. The ceramic window, being transparent to MW, allows the irradiation of the storage medium.

In the following, the characteristics of the storage tank models developed are described, followed by the results of the simulations performed.

2.3 Development of the CFD model

The models developed and studied in this paper are numerous and have slightly different characteristics. However, it is possible to make a general description of the characteristics common to all the models and, later, in the section dedicated to the results, specify the specific characteristics that each model presents and the reasons for certain choices.

First of all, it is important to reiterate that all the simulations performed are based on a thermocline TES model developed by ENEA and analysed in the previous section. Therefore, the basic concept of the reservoir operation remains unchanged, although some important changes have been made. In particular, the main development that has been made in this work concerns the implementation of a device that allows the heating of the molten salt by MW irradiation.

All models were designed and drawn using SolidWorks software, while fluid dynamics simulations were performed using STAR-CCM+ software. The use of software in the fluid dynamics field allows to predict with high accuracy and with a relatively low computational cost the behaviour of fluids in both laminar and turbulent flow. In particular, STAR-CCM+ allows to numerically solve, thanks to iterative methods, the Navier-Stokes equations, dividing the computational domain into many control volumes. For each control volume, the momentum and energy conservation equations are solved iteratively, producing as output the three components of the velocity along the Cartesian axes and the temperature. In this way, it is possible to know the velocity and temperature field at each point of the domain. Finally, it is also possible to study the behaviour of fluids in non-stationary applications, the transients (such as the charging and discharging phases of the storage) by defining a time-step.

2.3.1 Computational domain

In this section, the computational domain and the main assumptions adopted are exposed. The models created in this thesis, as it will be explained in more detail, have slightly different geometries, since some components, in some configurations, have been modified to improve the performances of the temperature stratification (TS) inside the tank. However, most of the components remain unchanged in all the simulations. The major innovation concerns the implementation of the device for the microwave heating inside the tank. In this sense, two different types of configurations, Configuration A and B, have been designed, which have two different geometric shapes to discharge the radiative energy.

In the following, the main geometric details of the elements that make up the storage tank are described. Furthermore, since some components present in the geometric design have not been considered in the fluid dynamics simulation (for example, the wall of the central channel), it is indicated which of them are actually included also in the simulations. In these cases, the components are replaced by empty volumes in STAR-CCM+.

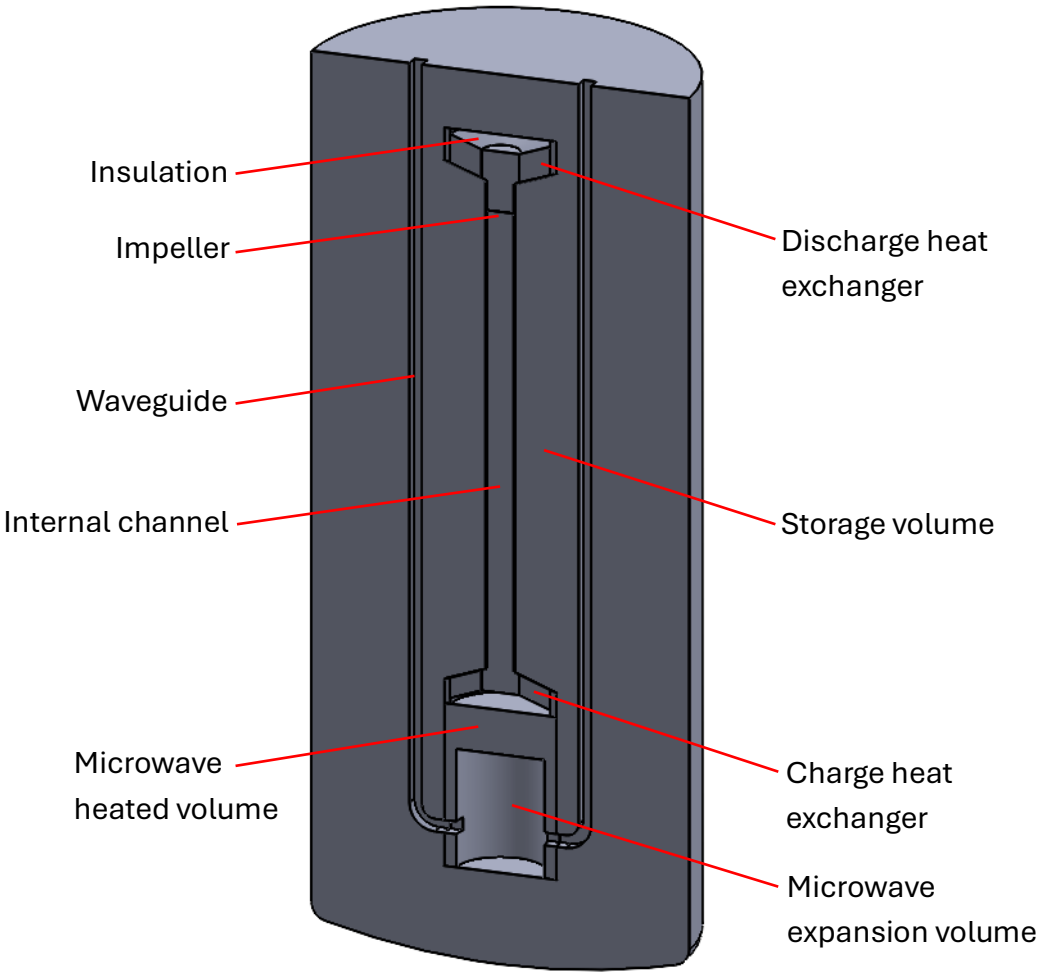

Figure 17 - CAD representation of the main components (Configuration A)

Below there is an exhaustive description of the components:

- Storage volume: the domain considered in the modelling of the problem includes the internal volume of the storage tank occupied by the molten salt and the components that make up the central channel. Consequently, the external steel vessel and the insulation were not considered in the model and were replaced by specific boundary conditions. Similarly, the upper part of the container, above the surface of the molten salt, consisting of a layer of air and the steel cover (where valves and flanges are present), was replaced by the boundary conditions. The total height of the internal volume occupied by the molten salt was increased to approximately 3 m to allow for the insertion of the MW heating device. The internal radius of the tank vessel, however, remained unchanged, measuring 642 mm.

- Internal channel: the channel through which the molten salt rises/falls during the charging/discharging phases is 1650 mm high (without considering the height

occupied by the heat exchangers). The external diameter of the channel is 101.6 mm and the internal diameter is 45.06 mm. The steel tube was neglected in the fluid dynamics simulation, thus considering the heat exchange between it and the surrounding volume of MS to be zero.

- Microchannels (MC): as it will be seen later in the section dedicated to the results, in some cases the central channel has been replaced by microchannels with a diameter of 10 mm for a total length of 1 m. This choice is due to the need to reduce the flow rate circulating in the central channel by increasing the hydraulic impedance of the channel. In fact, the microchannels cause concentrated pressure drops near the inlets and outlets in addition to the distributed pressure drops along the entire length over which they extend. The pressure drop caused by the MC causes a decrease in the flow rate in the central channel, thus decreasing the effect of the recirculation of salts in the tank. This aspect results in an improvement in temperature stratification. During this work, different configurations were tested, which present a different number of MC. In particular, configurations with 4, 7, 13, 19, 25 microchannels were tested. The MC are arranged on 1, 2 or 3 concentric circles in a symmetrical manner. The arrangements inside the central channel is shown in the following figure.

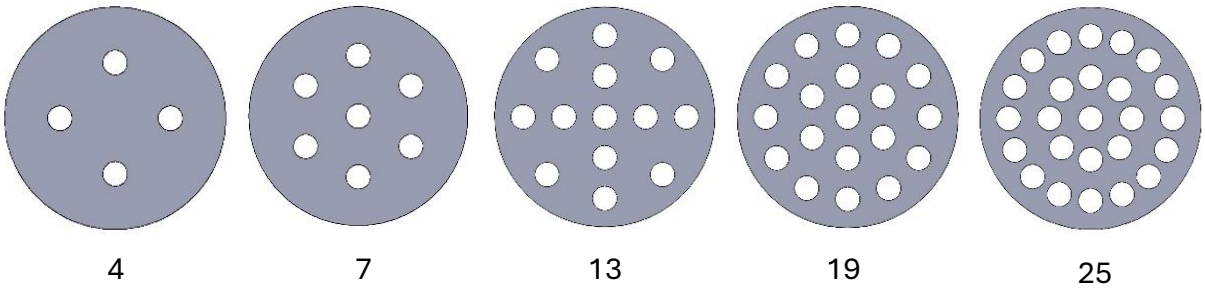

Figure 18 - Microchannels arrangements

The following figures show an example of how the microchannels were inserted into the storage tank, to make their arrangement clearer.

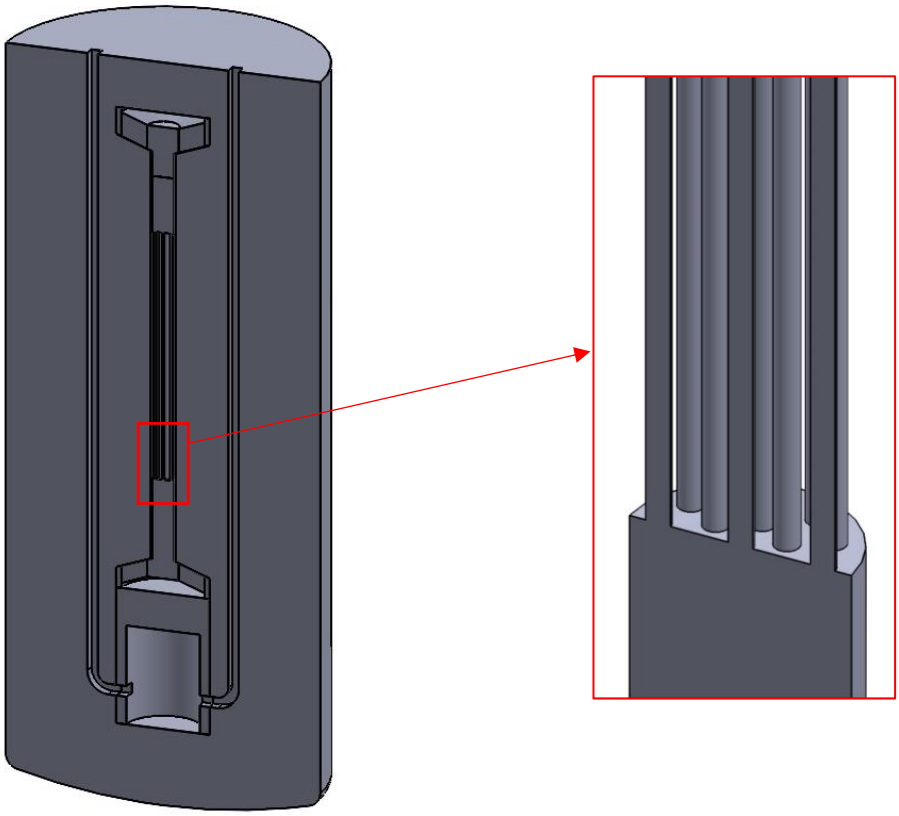

Figure 19 - Microchannels CAD representation

- Heat exchangers (HXs): the areas occupied by the heat exchangers, i.e. the upper and lower parts of the channel, are made up of an enlargement of the central channel, which takes on the shape of a truncated cone with a side surface inclined at 20°. The coil of tubes that makes up each heat exchanger has been neglected because, as explained later, it has been replaced by a porous medium in the fluid dynamics simulation.

- Insulation: in the part below the charge HX and the part above the discharge HX there are volumes occupied by insulation. They also have a truncated cone shape and are necessary to avoid stagnation of the fluid in these areas. In fact, in particular with regard to the lower insulation, The heat source is located below the part occupied by the insulation, and if the latter were not present, the fluid would stagnate and potentially reach too high a temperature. The two volumes occupied by the insulation have been neglected in the fluid dynamics simulation.

- Microwave heating device – Configuration A: the microwave heating device is positioned in the part below the internal channel. In continuity with the wall that constitutes the entrance to the internal channel, there is a hollow cylinder arranged on the central axis of the tank with a thickness of 2 mm, an external radius of 192 mm and a height of 550 mm. Inside the cylinder, there is a cylindrical volume with a radius of 150 mm and a height of 400 mm occupied by air. This last cylinder is necessary for the expansion of the microwaves, since, according to recent studies conducted by ENEA, the presence of a volume of air that is placed between the waveguide and the molten salt allows for better heating performance. In fact, the volume of air allows for better uniformity of the electric field and more efficient heating of the salts. The upper part of the cylinder is made of a ceramic window, which, unlike steel, is invisible to the electromagnetic field at microwave frequencies. In this way, the microwaves irradiate and heat up only the part above the expansion air cylinder. The MW, produced outside the tank, are transported along 2 rectangular section waveguides of the WR340 type, with a section of 86.36mm x 43.18 mm. The waveguides follow a vertical path from the upper part of the tank, making a 90° curve to reach the MW expansion air cylinder. The volume occupied by the expansion cylinder and the waveguides is not included in the domain of fluid dynamic simulations.

- Microwave heating device – Configuration B: The operating principle of the microwave heating device in Configuration B is similar to that of Configuration A. In fact, the hollow outer cylinder and the waveguides are the same as those of Configuration A. On the contrary, the main difference between the two configurations is the expansion cylinder. In fact, in Configuration B, there is an expansion volume (occupied by air) that has a section of an annulus. In this way, the flow of molten salt flows in the central channel of circular section. The microwaves, after expanding in the air volume, discharge their radiative energy through the internal ceramic wall of the cylinder with the annulus section. The channel through which the molten salt passes has been calculated to have the same section area as Configuration A, resulting in a radius of approximately 116.5 mm. Again, the entire microwave heating device is not included in the fluid dynamics simulation.

- Impeller: to simulate the operation of the impeller inside the central channel, an interface called “fan interface” was inserted in some simulations. This type of interface allows to impose a forced pressure drop. In fact, it is sufficient to insert a polynomial characteristic curve of the pressure drop as a function of the flow rate circulating in the channel. In this paper, it was decided to test some configurations with fan interfaces with a constant characteristic curve, therefore the pressure drop

remains constant as the flow rate varies. However, as it will be highlighted later, the results were not satisfactory.

2.3.2 Simulation physics

In this subsection, the physics assumptions adopted in the models are described. In particular, the main characteristics of the elements introduced in the models on the STAR-CCM+ software and the main simplifications are described below:

- The fluid used in the simulations in this paper is a mixture composed of 60% sodium nitrate and 40% potassium nitrate, also called “Solar salt”. This type of mixture can be used in the temperature range between 533 K and 894 K. In fact, at temperatures lower than the operating temperatures, the crystallization and solidification of the salt occurs, while at higher temperatures it loses its properties with the release of nitrites. On the STAR-CCM+ software, it is possible to set the properties of the liquids by defining their main physical properties, such as density, specific heat, thermal conductivity and viscosity. These properties are entered in the form of polynomial functions described in (Ferri R., 2008).

- In all simulations performed, the Boussinesq approximation is used, which represents a solution widely recognized as valid by the scientific community in the case of natural convection problems, having an excellent response to experimental data (Barletta, 2022). Natural convection is the phenomenon that, in a system, determines the movement of the fluid caused only by heating in a stable gravitational field. This simplification allows us to consider the density constant everywhere in the mass, momentum and energy conservation equations except for the source term in the momentum conservation equations (Lappa, 2022). This term, in the case of natural convection, is linked to the gravitational force.

- In the simulations the flow model is considered laminar. This choice is mainly due to the flow regime present in the tank volume. In fact, internal motions can be divided into laminar, transitional and turbulent motions. The difference between the various motions is due to the type of fluctuations and vortices present in the motion. In laminar motion, there are no fluctuations and the velocity can be considered one-dimensional. In turbulent motion, however, large fluctuations are present and the velocity has components in all directions. The transitional state is characterized by small fluctuations. To make the study of internal motions more precise from a quantitative point of view, the most common way to characterize an internal motion is the calculation of the Reynolds number, i.e. the ratio between the inertial and

viscous effects in the flow (Munson B. R., 1995). The Reynolds number is directly proportional to the velocity (therefore, to the flow rate) and to the size of the passage section. On the contrary, it is inversely proportional to the viscosity. In the simulations performed in this work, the fluid velocity is very low in the volume of the tank, with an almost stationary regime. Instead, in the central channel, it has been calculated that in some configurations the flow reaches states of slight turbulence, even if in most cases the regime is transitional or laminar. For this reason, it was decided to use the laminar model, since it better represents the state of motion inside the tank.

- The charging and discharging HX(s) in the central channel are modeled as porous media. This choice is due to the fact that the objective of this paper is to evaluate the heating carried out by microwaves, so the charging and discharging coils are considered as passive media through which the fluid flows. The choice of using a porous medium significantly simplifies the geometric complexity and the computational cost of the simulations. The accuracy of the use of porous media instead of coils has been verified in a previous studies developed by ENEA. In the STAR-CCM+ software, the porous medium is modeled according to the Darcy equation and subsequently modified by Forchheimer. This equation allows to estimate the pressure drop through a porous medium as a function of the fluid velocity. The equation depends on some fundamental parameters that must be specified when defining the porous medium, namely the porosity (from which the fluid filtration velocity is calculated), the Forchheimer coefficient and the permeability coefficient. In particular, through the Forchheimer coefficient it is possible to take into account the inertial effects, not considered in the original equation proposed by Darcy (Sobieski W., 2014).

- The method of solving the mass, momentum and energy conservation equations varies according to the sequence of the resolution of the discretized equations. The two methods implemented in the software are the *segregated* one, in which the equations are solved sequentially one after the other, and the *coupled* one, in which the equations are solved simultaneously. In this work, the segregated method is used exclusively, since it is more suitable in cases where large velocity gradients are present, as in the case of internal flows (for example in pipes and centrifugal pumps). On the contrary, the coupled method is generally used for supersonic and hypersonic flows, in which shock waves with large pressure and density gradients are generated (Alonzo-García A., 2016).

- The method used to model time is the *implicit unsteady* one. In fact, the charging and discharging of the storage tank require the resolution of a transient problem in order to evaluate the temperature trend at each point of the domain for a given period of time. The implicit method is generally chosen instead of the explicit method because it is unconditionally stable, It therefore allows the user to define a time step according to the needs of each problem. Instead, the stability of the explicit method depends on the size of the mesh cells. For this reason, the explicit method is used when the time interval of the transient is relatively short, otherwise it can cause excessively high computational costs due to the need to define a time-step that is too small (Venkatakrishnan V., 1996). In the simulations carried out in this project, the time-step was defined as 5 seconds.

- Since the aim of this work involves the study of the charging process of thermocline storage, it is necessary to define an initial condition at which the molten salt is found. In the simulations carried out, it was decided to set this temperature to 290 °C (563 K). This choice is due to operational issues of management of CSP plants, since, although the melting temperature of Solar salt is around 260 °C, in real plants it is preferable to maintain a safety margin to avoid any localized freezing.

2.3.3 Boundary conditions

One of the most important operations in fluid dynamics simulations is the definition of boundary conditions. They represent the physical conditions in which the boundaries of the computational domain are described. Through boundary conditions, the problem becomes completely defined and the software can iteratively solve the conservation equations within the domain. The boundary conditions adopted in the simulations are described below:

- Molten salt-air interface: the upper wall of the computational domain, corresponding to the interface between the molten salt and the air layer inside the tank, is modeled as follows. The surface, despite being an interface between two fluids, is modeled as if it were a solid wall. First, the “slip” condition of the tangential stress is imposed on this surface. This condition allows the upper wall to be modeled as if it were free to move, canceling the tangential stress. In this way, the condition of the interface between two fluids becomes reasonably realistic. From the point of view of heat exchange, as described in the report realised by ENEA (Cagnoli M., 2023), a heat flow with a linear characteristic depending on the temperature of the salts on the interface is imposed on the upper wall. To calculate the heat flow imposed on the interface between salts and air, a special 3D model that represents

the upper part of the tank was created, including the air layer, wall, external insulation and flanges. Subsequently, a parametric study was carried out, varying the temperature of the interface between salts and air and measuring the heat flow lost. The calculations consider environmental conditions of 15 °C of external temperature and 5 m/s of wind speed. As an example, at a temperature of 290 °C, i.e. the initial temperature at which the salts are found during the charging process, the heat losses through the upper wall are approximately 180 $\mathrm{W/m^2}$.

- Side wall and bottom wall heat losses: in this case too, the external walls and the insulation layer that surrounds the tank are replaced in the model by imposed conditions of heat flow. In this case, the boundary condition "convection" can be inserted in the software, thanks to which the software calculates the convective heat losses of a given surface. To define the conditions that describe convection in the software, it is necessary to obtain a heat exchange coefficient and the ambient temperature, which is set at 15 °C. The heat exchange coefficient is a parameter that takes into account the thermal resistances of the tank wall (R_{wall}), of the insulating layer (R_{ins}) and convective heat exchange with the external environment (R_{conv}) and the wall surface (A) (Cagnoli M., 2023), according to the formula:

$$h_{eq} = \frac{1}{(R_{wall} + R_{ins} + R_{conv}) \times A} \qquad (55)$$

  To evaluate the convective resistance, it is necessary to use semi-empirical correlations, among which the well-known Churchill-Bernstein correlation is used (Incropera F. P., 1996), used for the side wall of the tank, while the bottom wall is considered a flat plate. Considering a molten salt temperature of 285 °C and environmental conditions identical to those described above, the heat exchange coefficients obtained are equal to 0.51 $\mathrm{W/m^2}$ for the side wall and 0.45 $\mathrm{W/m^2}$ for the bottom wall.

- Symmetry planes: since the tank has two symmetry planes passing through the central axis and perpendicular to each other, it is possible to reduce the computational domain to 1/4 of the real tank. This solution allows to significantly reduce the computational cost, while maintaining the same accuracy. Therefore, on the surfaces that lie on the symmetry planes, the boundary condition called "symmetry plane" is imposed, which allows to apply a mirror-symmetry condition on a structure.

- Volumetric heat source: to simulate microwave heating, it was decided to impose a uniform volumetric heat source in the volume of molten salt near the device

dedicated to MW heating. This choice is due to the fact that it is not yet possible to obtain valid simulations of the behaviour of molten salt when irradiated by microwaves, since the dielectric properties have not yet been adequately studied. For this reason, it was decided to use a uniform volumetric source, considering that the expansion of the microwaves in the air volume can make the irradiation of the salts as homogeneous as possible. In the case of Configuration A, the volume subject to the volumetric heat source is represented by a cylinder located above the microwave expansion cylinder. In fact, the microwaves, being reflected by the steel walls, can irradiate the volume of salts only through the flat ceramic window located in the upper part of the cylinder. In Configuration B, however, the ceramic window has a cylindrical shape and the microwaves heat the cylindrical volume towards which the window faces.

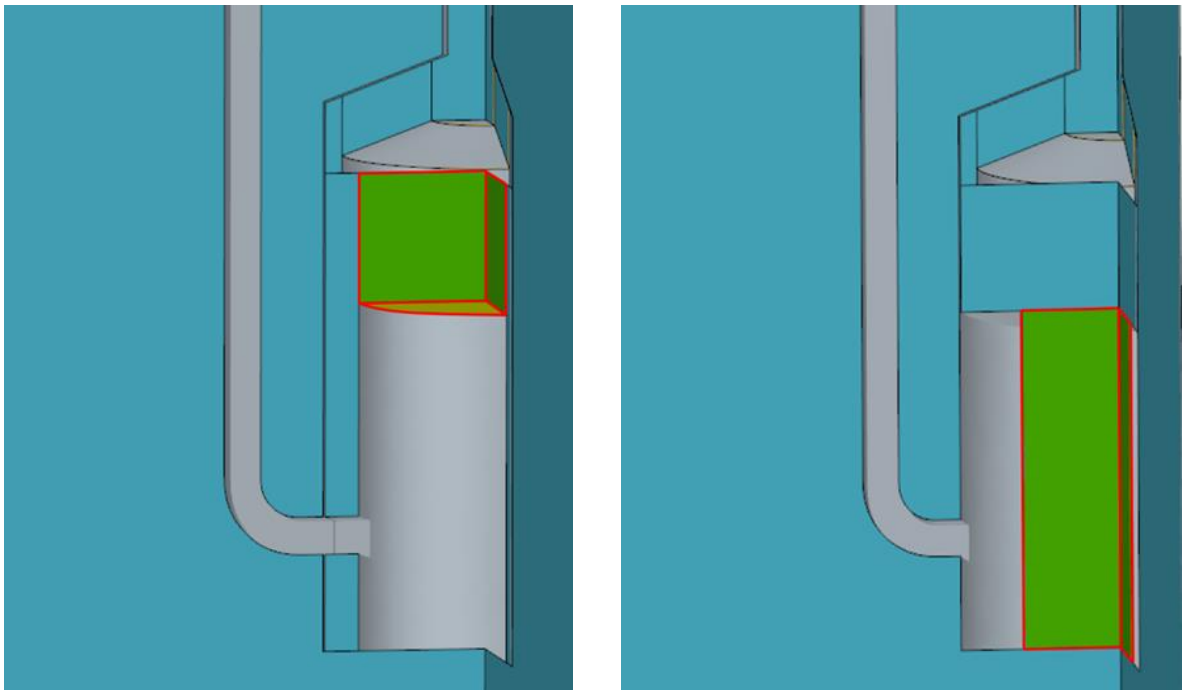

Figure 20 - Volumes heated by the volumetric heat source: Configuration A (left) and Configuration B (right)

2.3.4 Mesh generation

The definition of the computational mesh is the subdivision of a continuous geometric space into discrete geometric cells. The need to divide the domain into numerous discrete volumes is due to the fact that the conservation equations are solved numerically in an iterative manner within the software (not being possible to solve them analytically). Therefore, the software for each control volume or cell solves the conservation equations iteratively. For this reason, dividing the domain into a higher number of elements allows to obtain a more accurate solution and more similar to the ideal solution of the continuous volume.

The discretization of a continuous space represents a delicate and fundamental step in CFD simulation and resolutions. In fact, in the case in which the generated mesh is insufficiently fine or excessively fine in some areas or in the entire domain, the solution could be inaccurate or wrong. For this reason, it is necessary to follow precise criteria in order to generate an adequately fine mesh in every part of the computational domain to have an accurate and reliable solution. The main characteristics used to generate the computational mesh are described below. The main parameters used to define the size of the cells and refine the mesh will be exposed later.

First of all, the first fundamental step concerns the choice of the core volume mesher, that is the model used to generate a volume mesh. The core volume meshers available on STAR-CCM+ are three:

- Tetrahedral: this type of mesh uses tetrahedral shaped cells. This model represents a simple solution for the generation of complex meshes. The amount of memory occupied by this type of mesh is the smallest, given the same number of cells, compared to the other two methods.

- Polyhedral: this type of meshing uses cells of arbitrary polyhedral shape. The cells have on average 14 faces. This type of meshing is relatively easy to build and requires about 5 times fewer cells than the tetrahedral mesh from the starting surface.

- Trimmed: this type of mesh is mainly made up of hexahedral shaped cells, reducing the cell skewness. It represents an efficient and robust method for creating high quality meshes for simple and complex meshes.

The choice of the model has a great influence on the subsequent accuracy and order of convergence of the solution. In fact, although the tetrahedral mesher is the solution that requires less space occupied in memory and is faster in generating the mesh, it requires 5 to 8 times the number of cells compared to the trimmed and polyhedral meshers in terms of solution quality. Therefore, in general, using trimmed or polyhedral meshers the quality of the solution is higher. In this work, given the considerations just made, it was decided to use the polyhedral mesher.

Furthermore, it was decided to insert the “prism layers”, that is orthogonal prismatic cells next to wall surfaces or boundaries. These layers of cells are necessary to obtain a more accurate result near the edges of the domain, since in these areas there is the greatest velocity gradient (due to the no-slip condition that imposes a zero velocity on the edges) and often great temperature gradients. The prism layers are particularly important in the case of turbulent flows, however they make the result more reliable even with laminar motion. In this work it was decided to insert 4 prism layers, which have a total thickness of 5 mm.

The parameters used to define the mesh are numerous, so it was decided to describe only the main ones. The most important parameter is undoubtedly the “base size”, that is the characteristic size of the cell. The base size represents, on average, the distance between two opposite faces in each cell. After a study of the solution independence with respect to the mesh size, it was decided to use a size equal to 6 cm, since it allows to reach a high accuracy of the solution while maintaining a reasonable computational complexity. This solution allows to obtain a mesh composed of 76716 cells. The results of the mesh independence study are summarized in the following plot, considering the relative error on the mass flow rate measurement inside the internal channel after 600 seconds.

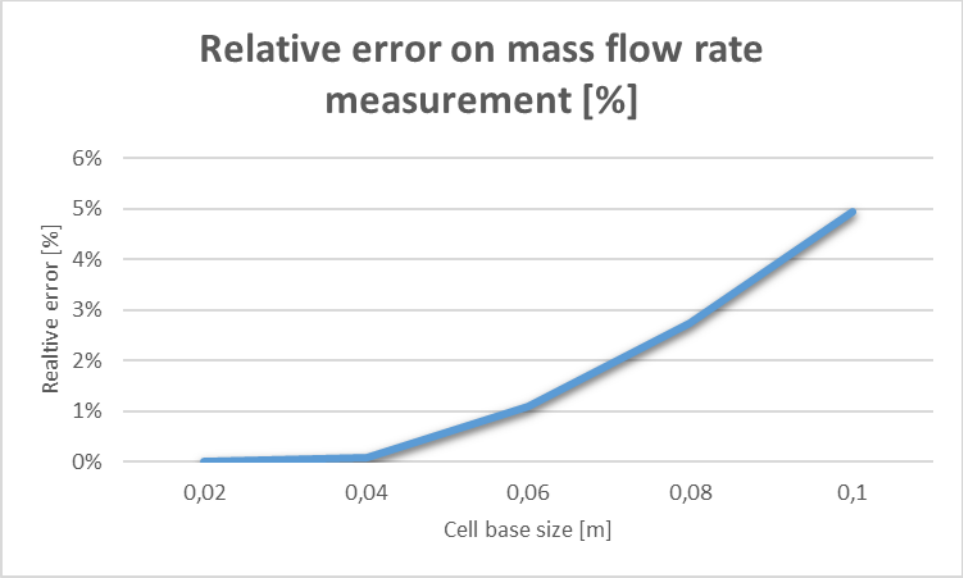

Figure 21 - Mesh independence study

Although cells are described by a characteristic size, in reality, most cells have smaller dimensions. In fact, using the “surface growth rate” parameter, it is possible to create a mesh that has increasingly larger cells moving away from the surface of the edges, until reaching the nominal size far from them. In this way, the areas close to the surface are refined more, increasing the accuracy of the solution. In this work, a surface growth rate of

1.3 was decided to use. It is also possible to define a growth rate for the prism layers, which has been set to 1.5. In the following pictures, the generated mesh is shown.

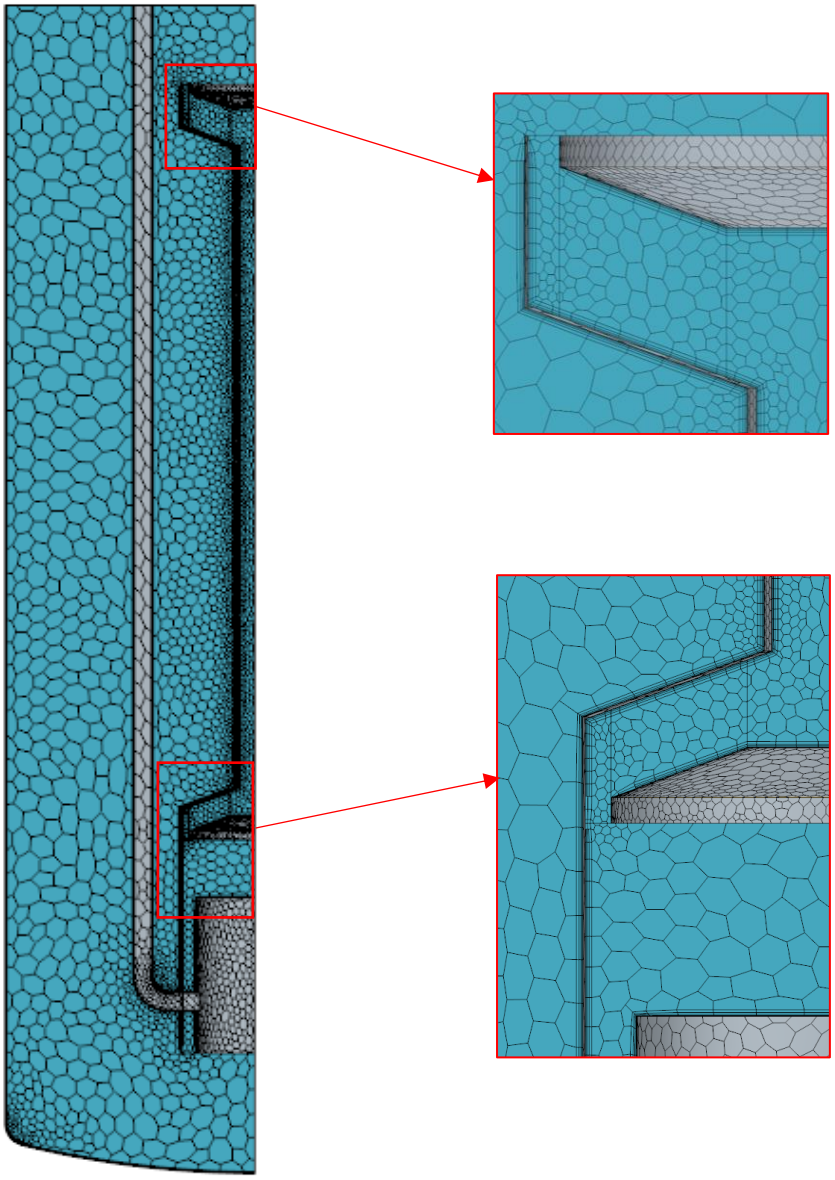

Figure 22 - Mesh generation

2.4 Simulation results

In this section, the results of the simulations performed are described and discussed. Before describing the simulations, it is necessary to give an overview of how the project was carried out and what were the main choices that led to the implementation of further changes to the configurations.

First of all, the study that was carried out in the simulations always concerns the storage tank charging transient, in order to study the temperature at various points of the tank, the flow rate circulating in the channel and other useful parameters. During the transient, the power injected into the heated volume is constant over time. Furthermore, in general, the duration of the charging transient is studied for a time interval of 60 minutes.

The development of the experimental simulations on the STAR-CCM+ software was conducted in three phases. In the first phase, the charge transient in the case of microwave heating is studied for both Configuration A and Configuration B. After the first phase, given the low level of stratification obtained inside the storage tank, it was decided to impose a localized pressure drop inside the central channel, using the “fan interface” model explained in the previous chapter. Since in the first phase the results obtained in the two configurations were almost identical, it was decided to proceed with the simulation of Configuration A only from here on. In the third phase, given the unsatisfactory results obtained through the use of the “fan interface”, we proceeded with the insertion of microchannels in the central channel to introduce a localized pressure drop inside the channel thanks to the geometry variations.

2.4.1 Charge simulations for Configurations A and B

In this first part of the results section, it was decided to analyze the charging phase of the thermal storage in Configurations A and B. As previously described, the two configurations differ essentially in the location of the volumetric heat source, while maintaining the same total power and the same passage section in the two cases. The total volumetric heat

source introduced is equal to 190 kW (even though in the software it is set to 47.5 kW, since the domain is reduced to 1/4 of the real one due to symmetry). The flow is laminar and the Boussinesq approximation is used. The initial temperature in which the salts are found is equal to 563 K.

The following figure shows the temperature profile inside the tank after 60 minutes in both configurations.

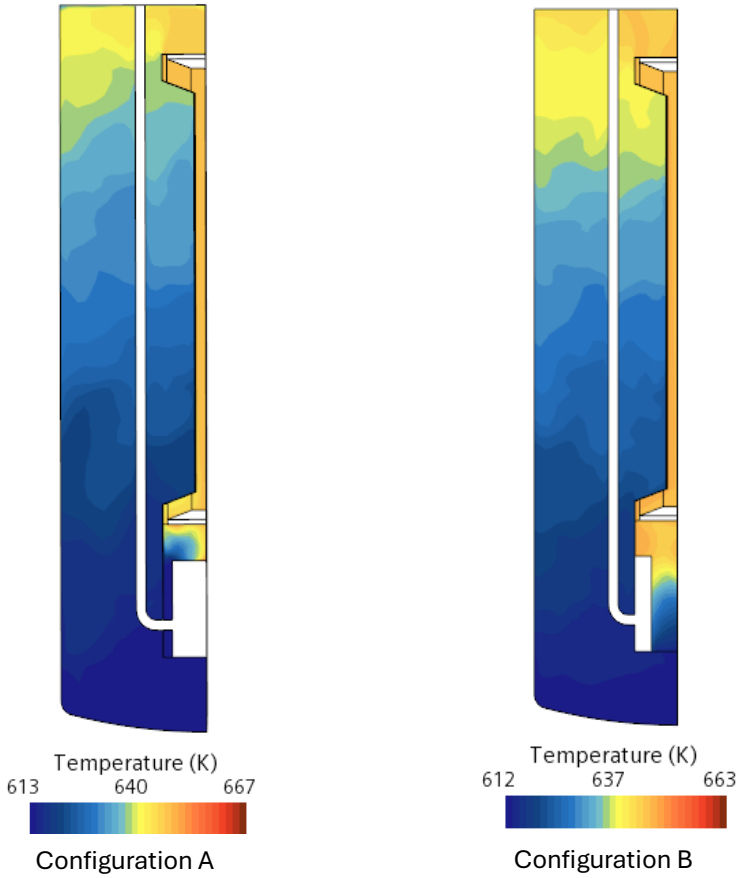

Figure 23 - Temperature distribution after 60 minutes charging transient: Configuration A (left) and Configuration B (right)

From the image, it can be seen that the temperature profiles in the two configurations are very similar, with only slight temperature differences. As previously explained, the molten salt is heated in the lower part of the tank in correspondence with the MW heating device. In fact, it can be seen how the fluid, once heated, rises along the channel until it reaches the upper part of the tank. It is also clearly visible that the temperature inside the channel is quite homogeneous, while in the storage volume there is a large temperature gradient. Although the central channel has operated successfully, it is noted, however, that the stratification is far from a perfect thermocline profile, in which there is a clear division

between the upper part at high temperature and a lower part at low temperature. For this reason, it was decided to study the thermocline profile, in order to understand the actual stratification profile.

To study the stratification in the tank, it was decided to monitor the temperatures inside the storage volume on equidistant horizontal surfaces. The number of surfaces considered is equal to 6, from the surface corresponding to the lower part (hereinafter, bottom or BTM) to the upper part (TOP). The same surfaces are also used in subsequent simulations. In the following picture, the surfaces where the temperature is measured are shown.

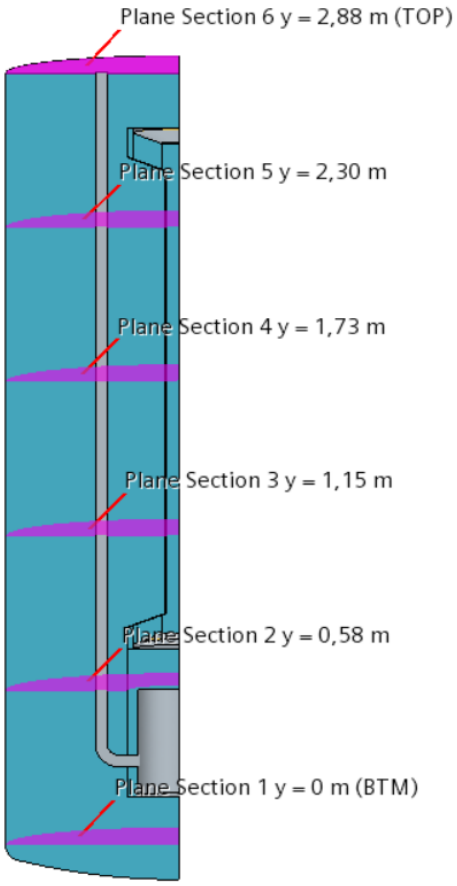

Figure 24 - Plane sections generated to monitor the temperature

As you can see, the surfaces, equidistant from each other, are characterized by a specific coordinate on the vertical axis, the y-axis. The following images show the trend of the temperature calculated on each surface shown in the previous figure during the transient measurement interval (60 minutes).

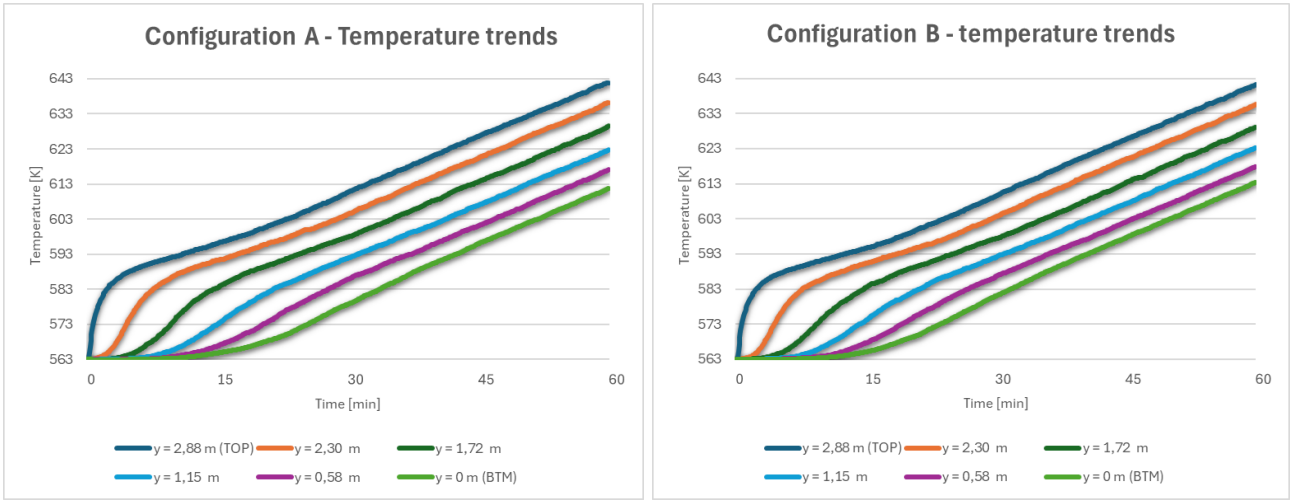

Figure 25 - Temperature at different tank heights during the charge transient: Configuration A (left) and Configuration B (right)

From the image, it can be seen that in the first phase, the temperature of the upper layer suddenly increases, while that of the lower layers remains almost stable. This trend suggests that the hot fluid, passing through the channel, has reached the upper part of the tank, replacing the upper layer of cold fluid. As a result, also the other layers later increase suddenly in temperatures, even though the steep rise is less pronounced for the lower layers. The phenomenon of stratification can be seen, which occurs from top to bottom in the volume of the tank. This phenomenon stops when a sort of stationary state is established in the tank in which all the surfaces increase their temperature in a constant manner (with the same derivative with respect to time). In this phase of the transient, the temperature difference remains constant between the various layers, but the temperatures increase, since the volumetric heat source continues to be present.

At this point, given that we have seen how a dynamic equilibrium is reached inside the tank, it is possible to study the profile of the thermocline, to understand what the temperature trend is on the vertical axis at a given moment. Therefore, knowing that the result is independent of the time instant considered, it was decided to show this result in the time instant equal to 3600 s, i.e. 60 minutes.

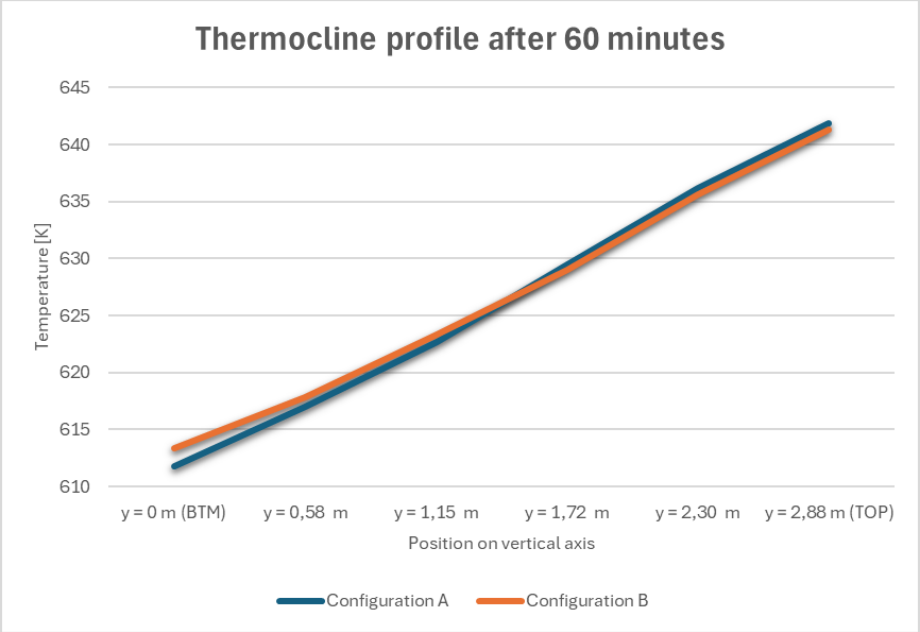

Figure 26 - Thermocline profile at time t=3600 s

The graph, as previously announced, shows the temperature profiles along the vertical axis of the tank in both configurations after 60 minutes. The temperature trend is linear, which shows how the stratification inside the thermocline is not optimal, since the gradient is constant, while the ideal situation involves a discontinuity that divides the upper part of the tank at high temperature from the lower part at low temperature. A very important aspect to underline is the almost superimposability of the two curves, which makes it even clearer how the two configurations lead to the same results. For this reason, in the next parts of the section dedicated to the results it was decided to carry out the simulations only on one of the two configurations, Configuration A.

From a quantitative point of view it is essential to make some considerations. The temperature difference between the upper and lower layer is approximately equal to 30°C in both configurations. Such a low temperature difference (TD) is absolutely insufficient and far from the objective for which the thermocline storage is designed in this thesis. In fact, since the tank is designed for CSP applications with the aim of avoiding the double tank system (one for the hot fluid and one for the cold fluid), the greater the temperature difference inside the tank, the greater the efficiency of the system. In fact, lower temperatures in the lower part increase the efficiency of the charging phase via CSP or microwave devices, while a higher temperature in the upper part allows a higher efficiency of the power generation system (based on the Rankine cycle). Therefore, it is essential to make the most of the operating temperature range of the MS, which, in the case of binary salts, varies between approximately 290 and 550 °C (although it is possible to reach temperatures up to 620 °C). Consequently, it is desirable to obtain temperature differences of around 200 °C in order to make the best use of the operability range of the molten salt. In

conclusion, it is necessary to make some changes to the system in order to increase the temperature stratification (TS) and obtain greater gradients.

2.4.2 Charge simulations for Configuration A with the impeller

In this second part of the results section, some changes have been made to improve the performance of the thermocline. In fact, as seen in the previous paragraph, the temperature stratification (TS) in the tank is not optimal and the temperature difference (TD) between the upper and lower parts is insufficient.

The TD is particularly low because the flow rate circulating in the channel is too high. In fact, the natural convection induced by the localized increase in temperature in the volumetric heating area is too high, causing excessive circulation of the fluid inside the channel. This excessively high flow rate also affects the volume of the tank, causing high mixing.

To deal with this phenomenon, it is necessary to make changes to reduce the circulating flow rate and thus reduce the mixing in the tank volume. In this part of the paper, it was decided to introduce an element that represents the axial impeller present in the real model designed and built by ENEA. It was, in fact, decided to introduce a particular type of interface, called "fan interface", which simulates the effect of an impeller. The fan interface is a type of interface that allows to introduce a localized pressure drop, defining a characteristic curve. The characteristic curve can be expressed in different ways, but in this work it was decided to introduce a constant pressure drop as the flow rate circulating in the channel varies. This choice is due to the need to decrease the flow rate circulating inside the channel, therefore treating the impeller as if it were a concentrated pressure drop. The following images show the place where the interface was placed.

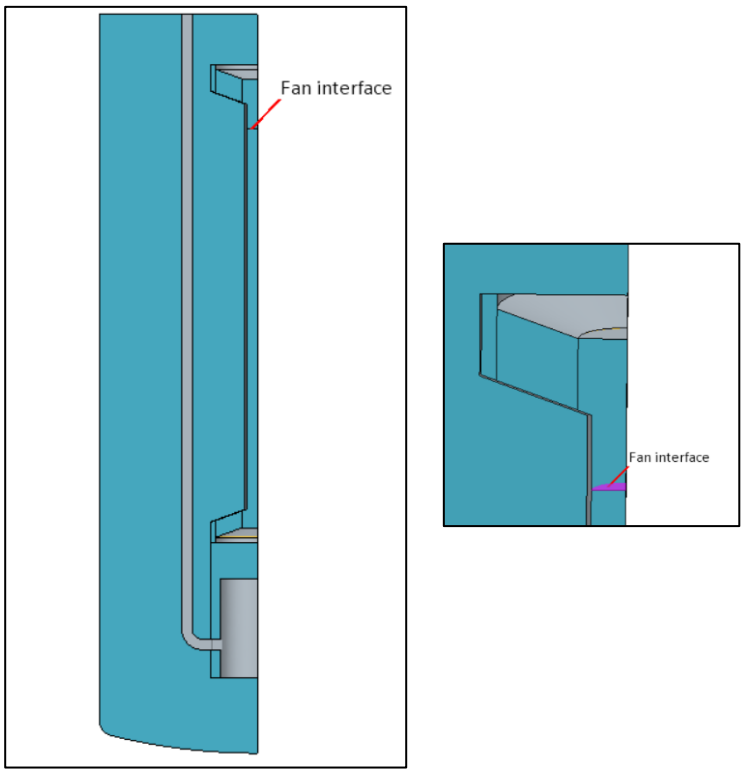

Figure 27 - Fan interface

The experimental simulations were carried out in this way: it was decided to impose ever-increasing pressure drops on the fan interface in order to decrease the flow rate circulating in the channel. Once the 60-minute transient was concluded, some fundamental parameters were analyzed, in particular the TD between the upper and lower layers of the tank and the mass flow rate circulating in the channel. As in previous simulations, the flow is considered laminar, the Boussinesq approximation is used, the total volumetric heat source is equal to 190 kW and the initial temperature of the salts is 563 K. The following images show the results of the simulations.

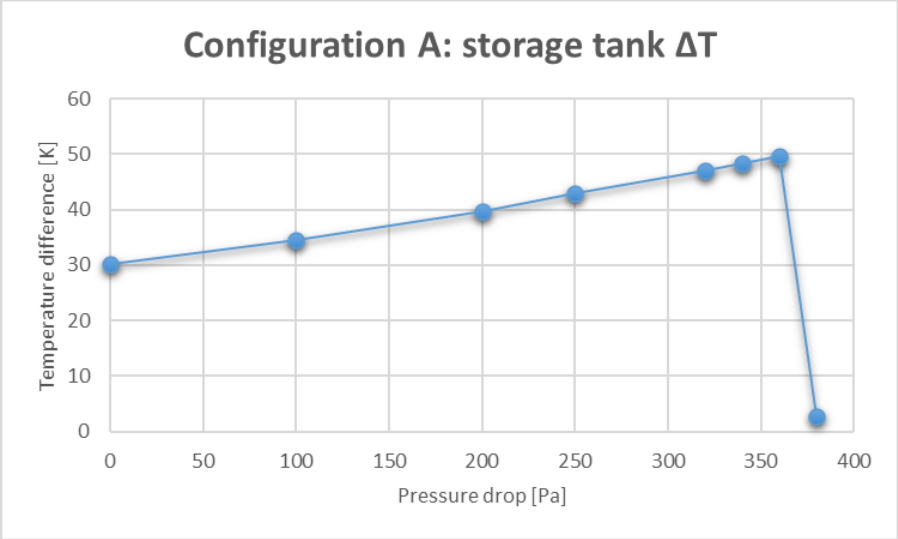

Figure 28 - Difference of temperature between tank top and bottom as a function of fan interface pressure drop

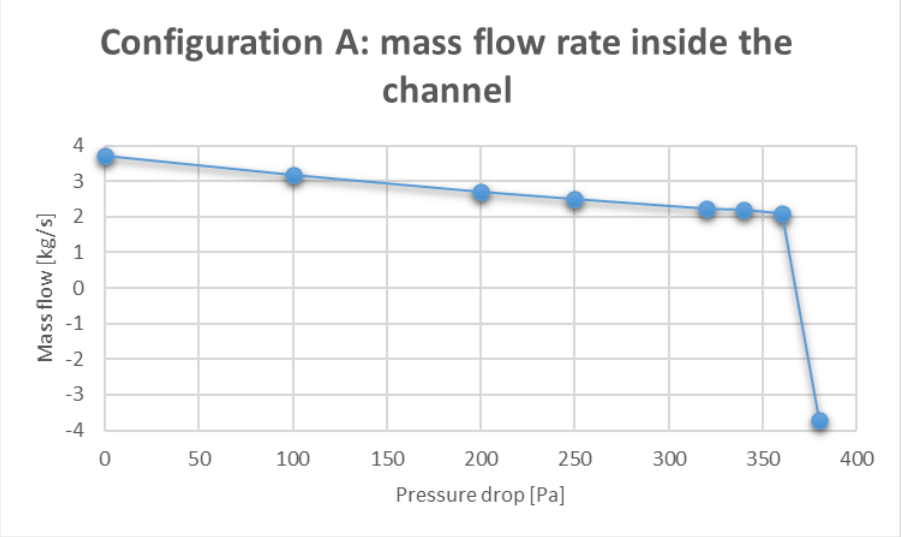

Figure 29 - Channel mass flow rate as a function of fan interface pressure drop

The previous figures show the trend of the TD and of the mass flow rate as the pressure drop imposed on the "fan interface" varies. The following characteristics can be noted from the graph:

- The trend of the TD (calculated as the difference between the temperature of the "Plane Section 6 (TOP)" and that of the "Plane Section 1 (BTM)" shown in the previous subchapter) at the instant t=3600 seconds is linear and increasing as the pressure drop on the interface increases. This result corresponds to expectations, given that by increasing the hydraulic impedance of the internal channel, the mixing of the fluid in the tank is lower.

- The mass flow rate circulating in the channel has a linear and decreasing trend as the pressure drop imposed on the interface increases. This is also an expected result, given that the pressure drop on the interface has the same physical meaning as a valve or a sudden obstruction to the movement of the fluid.

- The pressure drop imposed on the interface has a maximum limit beyond which no stratification is present. In fact, the maximum pressure drop to obtain a stratified temperature profile is equal to 360 Pa. Beyond this value, it can be seen how the stratification suddenly collapses. This aspect is particularly evident considering the mass flow rate, which assumes a negative value. This data indicates that the flow rate flows in the opposite direction, following the negative semi-axis of the vertical axis. The reason why this phenomenon occurs can be attributed to the fact that the "fan interface", in an attempt to hinder the passage of the fluid, beyond a certain pressure jump limit produces the inversion of the direction of the fluid, thus canceling the operating principle of the central channel and nullifying the stratification in the tank.

- The maximum value of temperature stratification in the tank, reached for an imposed pressure jump equal to 360 Pa, is approximately 50 °C. Although resulting in a clear improvement compared to the configuration without a fan interface, in which the temperature difference was about 30 °C, this temperature gradient is still far from the target to be achieved, i.e. about 200 °C.

- The minimum volumetric flow rate value achieved is about 2.1 kg/s. This value is significantly lower than the circulating flow rate without the implementation of the fan interface, i.e. about 3.7 kg/s. However, by carrying out a simple energy balance, it is noted that to obtain a theoretical stratification of 200 °C, the mass flow rate must be reduced to about 0.6 kg/s. This value, although remaining a quantitative reference,

would still not be sufficient, since it is calculated considering a perfect stratification in two distinct temperature values, while in reality it has been seen that there is a large gradient in the volume of the storage tank.

Given the above considerations, the results presented in this second part of the chapter, although better than those presented in the first part, are still insufficient and far from the final objective. For this reason, it is necessary to carry out further simulations, further modifying the system to improve the performance of the thermocline storage.

2.4.3 Charge simulations for Configuration A with microchannels

In this last part dedicated to the results, a new method was tested to try to improve the performance of the thermocline storage. In fact, in the previous simulations the results were unsatisfactory, given the low level of stratification inside the tank. Briefly summarizing, in the previous simulations the behaviour of the thermal storage during the charge transient was studied, with a constant volumetric power equal to 190 kW in the area where the MW heating device is located. In the first case, the tank configuration is the original one, therefore without modifications to the central channel, the stratification was insufficient. The temperature difference (TD) between the upper and lower part of the tank was just 30 °C. In the second case, with the introduction of a fan interface in the central channel that simulated the operation of an impeller, a temperature difference of about 50 °C was obtained. These results are unsatisfactory, since the operability range of the binary salts used in these simulations is between 290 and 550-620 °C. Therefore, it is physically possible to obtain much higher TD, close to 200 °C, which allow to exploit the temperature range much better, increasing the efficiency of the system.

The main reason that prevents a better temperature stratification (TS) in the tank, as previously mentioned, is the excessive flow inflow along the channel, which produces the mixing of the fluid in the tank. Consequently, in this section further modifications to the central channel have been tested in an attempt to improve performance. In particular, a part of the central channel has been replaced by microchannels (MC) with a diameter of 1 cm, inside which the fluid flows. The idea of introducing this system is to create a pressure drop in the channel, partially obstructing it, in order to decrease the flow rate. In fact, MC are characterized by concentrated pressure drops at the inlet and outlet, as described in (Munson B. R., 1995), due to geometry variations. Furthermore, there are also greater distributed pressure drops than in the case of a single channel, since there are more channels and the fluid, due to the law of conservation of mass, flows faster inside them. It should be underlined that the configurations with MC were tested without any fan interface.

The new configurations that have been tested with this type of implementation are five, with 4, 7, 13, 19, 25 microchannels inserted in the central channel. The arrangements in which the MC are inserted have been shown previously. As will be verified later experimentally, the number of MC is inversely proportional to the pressure drop caused. In fact, by decreasing the number, the passage section also decreases, producing a greater obstruction to the flow.

The simulations were carried out considering the following conditions. As in the previous simulations, also in these cases the storage charge transient is studied for a period of 60 minutes. The motion is laminar and the Boussinesq approximation has been used. The introduced power has been maintained equal to 190 kW and the initial temperature of the

fluid is 563 K. At the end of the simulations some parameters are studied. In particular, it was decided to study the TD of the fluid between the exit and the entrance in the volume heated by the volumetric source. Unlike the previous cases, where the TD was calculated between the layers at the top and at the bottom of the tank, this choice is due to the need to calculate the enthalpy jump provided to the salts without considering the thermal inertia of the total volume of the tank and the different temperature stratification for each configuration. In fact, the simulation results of these configurations present very different temperature stratifications in the tank and transient speeds, so the data of the temperature difference on the sides of the heat source makes the result more homogeneous. Furthermore, in addition to the temperature difference, it is important to study the mass flow rate circulating in the channel, to verify that the objective of introducing the MC (i.e. providing a pressure drop) is achieved. In the following pictures, the surfaces considered to measure the temperature differences are shown.

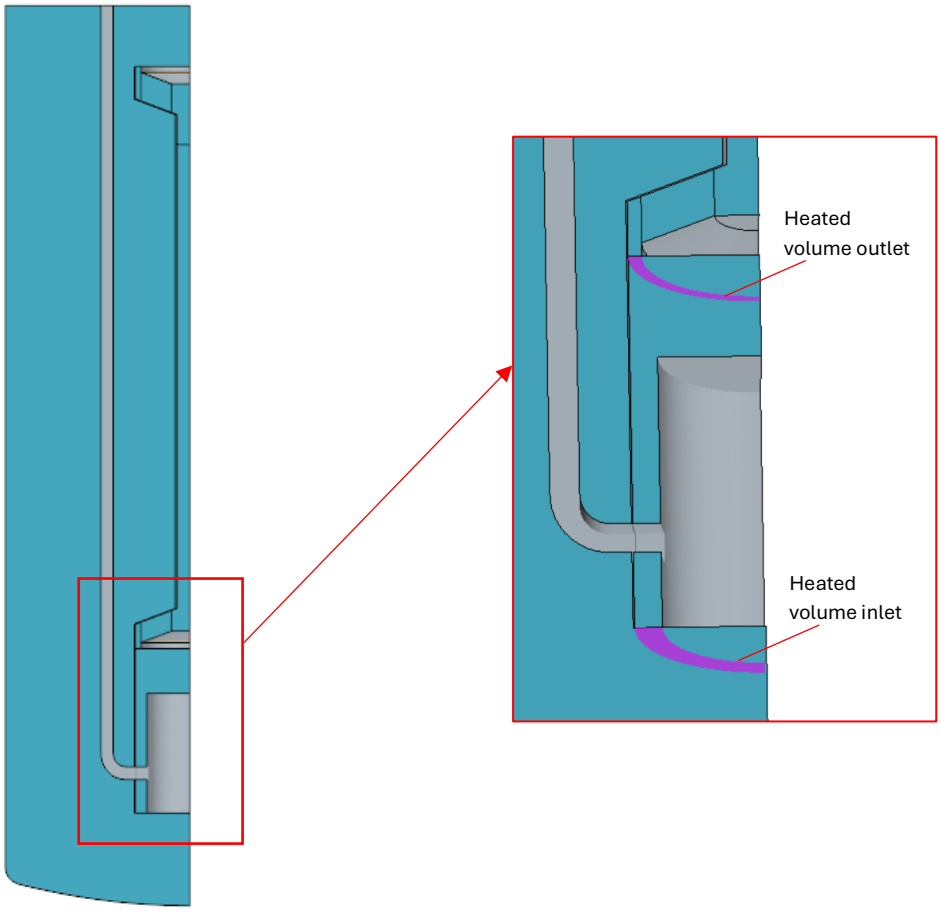

Figure 30 - Heated volume inlet and outlet

The following graph shows the results of the simulations performed by varying the configuration (therefore, the number of microchannels). The graph shows the TD between the outlet and the inlet of the heated volume and the mass flow rate circulating in the channel.

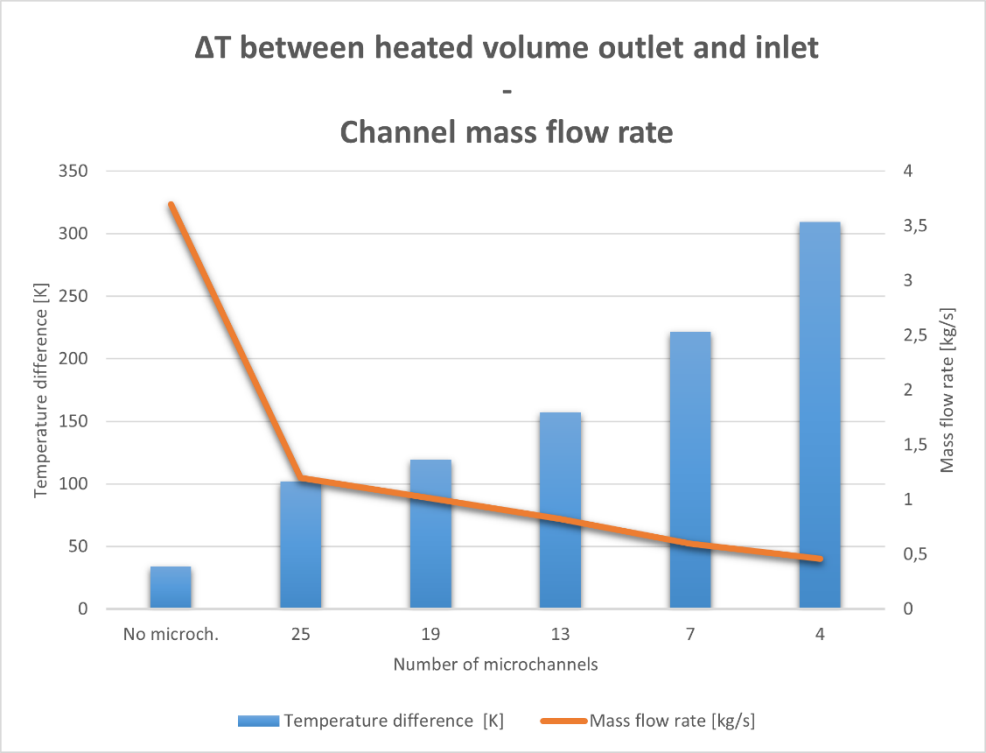

Figure 31 - Heated volume temperature difference and channel mass flow rate as a function of the number of microchannels

This graph is of fundamental importance to understand the operation of microchannel configurations. The following considerations can be made:

- The flow rate that flows in the channel decreases with the number of MC. This aspect corresponds exactly to the objective for which the MC were introduced. A clear decrease in the flow rate can be seen between the configuration without MC and the one with 25 MC. This aspect indicates that the pressure drop in the latter configuration is clearly greater, since the flow rate decreases from 3.7 to 1.2 kg/s. Subsequently, the decrease in the number of MC causes a more moderate decrease in the flow rate until it reaches less than 0.5 kg/s in the configuration with 4 MC. This aspect indicates, as expected, that by decreasing the number of MC and, consequently, of the passage section, the pressure drop increases, since the flow is more obstructed.

- The temperature difference between the outlet and the inlet of the heated volume is inversely proportional to the number of microchannels. In fact, the lower the number of MC, the lower the circulating flow rate and the lower the capacity to remove heat from the volumetric source. This effect implies an increase in the TD at the edges of the heated volume, causing a greater TD also in the storage volume. As it can be

seen, in the case where there are no MC, the TD is about 34 K, increasing up to 310 K in the case with 4 microchannels. This temperature difference is extremely high, which causes the maximum stability threshold of the salts (about 620 °C) to be exceeded almost immediately after the start of the transient. For this reason, this last configuration is not realistically applicable. On the contrary, in the case where there are 7 microchannels, the temperature difference is about 221 °C, which makes this configuration optimal. In fact, this configuration is able to make the most of the operating range of the fluid without damaging its properties for a long period of time during the transient.

The following table summarizes the fundamental data and the results of the simulations, since from now on, in the next figures they will be specified in the legend in order to simplify and make their understanding more immediate.

Table 1 - Main results from the simulations of microchannels configurations

Number of microchannels	Outlet/inlet heat source ΔT [K]	Channel mass flow rate [kg/s]	Volumetric heat source [kW]
No microch.	34	3.70	190
25	102	1.20	190
19	120	1.01	190
13	157	0.82	190
7	221	0.60	190
4	310	0.46	190

As mentioned above, the temperature differences are calculated between the outlet and the inlet of the volumetric heat source. However, it is important to note that this TD is close to an ideal system where a volume of fluid is completely heated from a lower temperature to a higher temperature. On the contrary, inside the tank volume such a clear separation between the hot fluid and the cold fluid is never present. In fact, there is always a large temperature gradient that makes the temperature difference between the top and the bottom of the tank non-ideal. Therefore, it is important to study also the TD inside the tank. The following image describes the trend during the transient of the

temperature difference between the upper and the lower layer of the tank with respect to time.

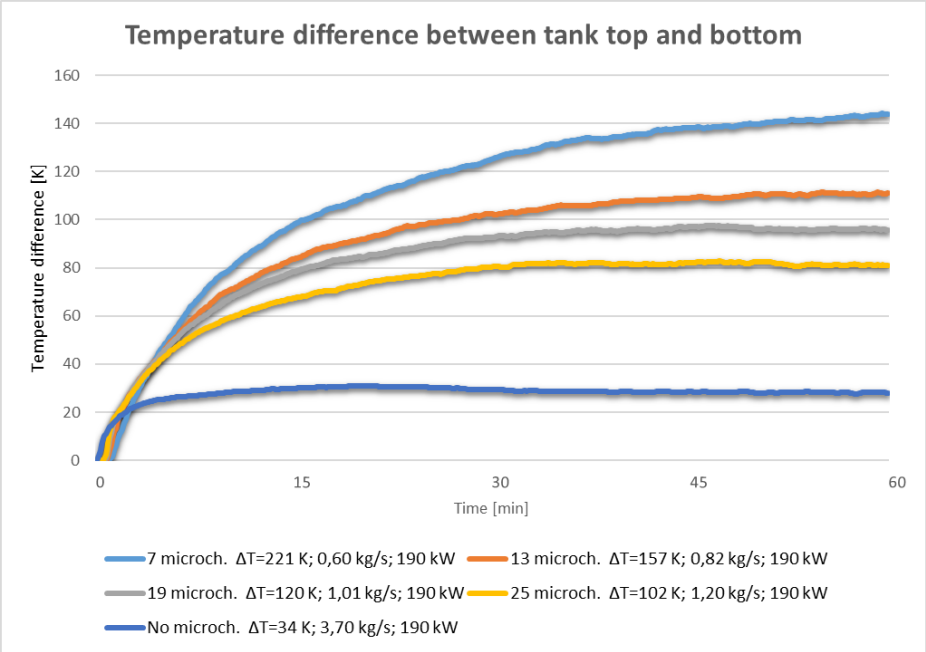

Figure 32 - Temperature difference between tank top and bottom as a function of time

As it can be seen, the temperature difference inside the tank has the same type of trend in each configuration. In fact, after an initial growth phase, at a certain point a quasi-stationary state is reached in which the TD in the tank stabilizes (while emphasizing that the absolute temperatures continue to grow). Another important aspect to consider is that the time taken to reach the stationary state is inversely proportional to the number of microchannels (and therefore to the flow rate that flows in the channel). In fact, by decreasing the flow rate, the stratification process slows down.

The most interesting aspect that can be deduced from this graph is, as mentioned above, the discrepancy between the TD between the inlet and outlet of the heat source and the TD in the tank. In fact, it is evident that the former is always greater than the latter, and this is due to the non-ideal stratification in the tank. The fact that there is always a thermal gradient in the volume of the tank generates temperature differences that are smaller than the ideal ones. For example, while in the case of the configuration without microchannels the discrepancy is a few degrees, in the case of the configuration with 13 microchannels the temperature difference across the heat source is 157 K, while across the tank it is approximately 111 K, so more than 45 K of difference.

At this point, since it has been assumed that a temperature gradient is always present in the tank and that the ideal state of the thermocline (in which there are two zones, one at a higher temperature and one at a lower temperature) is never reached, it is necessary to prove that this is actually verified by the experimental data. For this reason, to understand what the real stratification is, it was decided to study the temperatures on certain surfaces equidistant on the vertical axis, exactly as it was done in the first part of the section dedicated to the results. Even in this case, the instant of time in which the results were extrapolated is equal to 3600 seconds. The results are shown in the following plot.

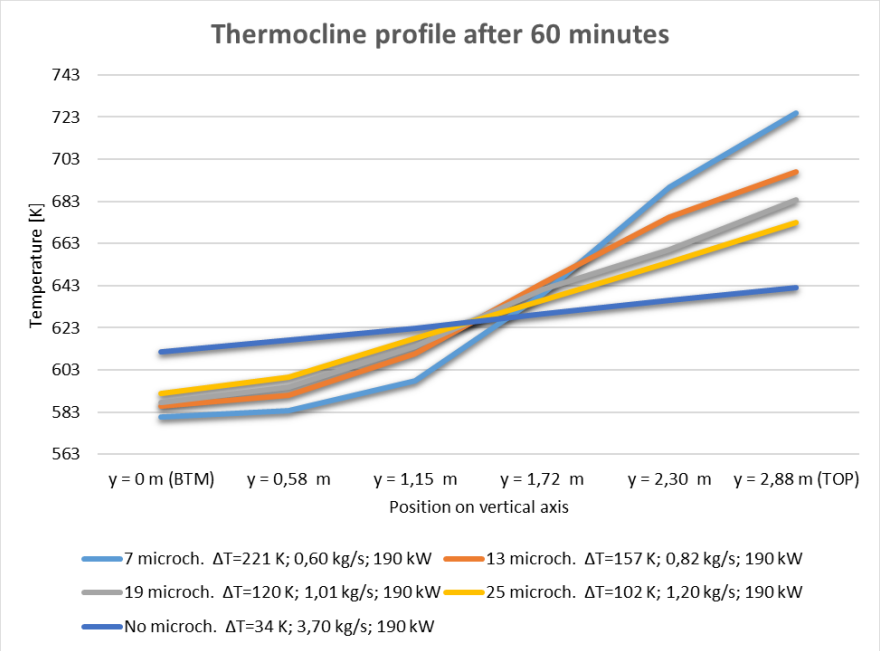

Figure 33 - Thermocline profile for each configuration at time t=3600 s

From the graph, it is clear that the temperature distribution profile along the vertical axis of the tank varies significantly in the different configurations. In fact, by decreasing the number of microchannels, a greater deviation from the linear profile obtained in the configuration without MC is noted. By increasing the hydraulic impedance of the central channel, not only there is a greater temperature difference obtained in the tank, but it is also possible to obtain better stratification. Furthermore, it is important to note how, in particular, in the configuration with 7 microchannels, there is a minimum temperature gradient in the lower layers. This aspect is important since in this way, the CSP charging coils can send fluid at a constant (and low) temperature to the solar field, increasing efficiency and decreasing thermal losses.

The next figure shows the temperature distribution in the storage after 3600 seconds for the configuration with 7 microchannels.

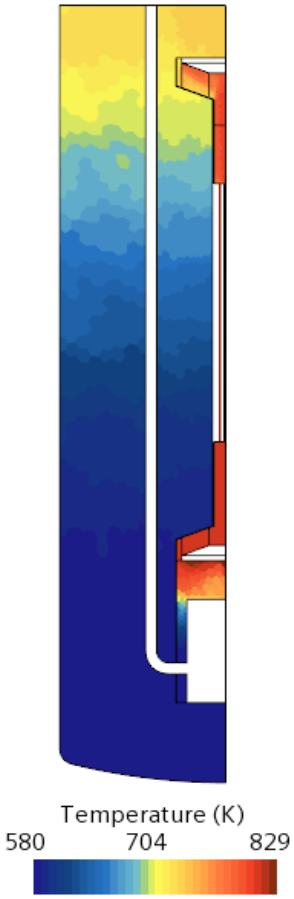

Figure 34 - Temperature distribution at time t=3600 s for the 7 microchannels configuration

After studying the thermocline profiles in all the configurations, it was concluded that the case with 7 microchannels was the most suitable, since, in addition to achieving an adequate temperature difference (making the most of the salts' operability range), it also presents the most efficient temperature gradient along the vertical axis.

In the following, an attempt is made to further improve the thermocline performance. From the previous considerations, it was noted that by decreasing the number of MC, the performance improves. However, the configuration with 7 microchannels seems to be a limiting case, since by further increasing the hydraulic impedance of the channel excessive values of temperature difference are obtained. In fact, in the case where only 4 microchannels are implemented, the TD exceeded 300 °C. It was decided to use the configuration with 4 microchannels and lowering the power of the volumetric heat source, in order to obtain lower temperature differences. In particular, it was decided to lower the power in order to obtain a TD between the outlet and inlet of the heat source

exactly equal to the case with 7 microchannels with nominal power (190 kW). The simulation result is shown in the following figure.

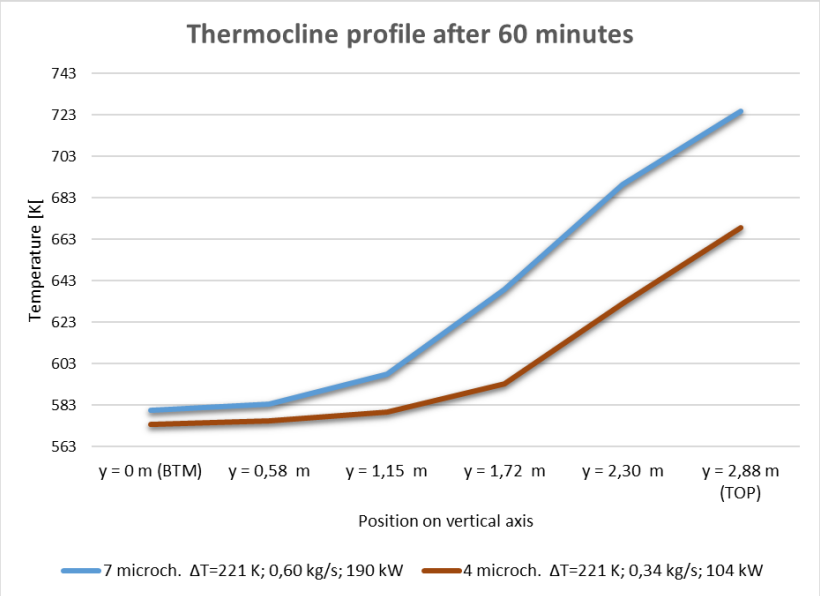

Figure 35 - Comparison between the 7 microchannels configuration at nominal power and the 4 microchannels configuration at reduced power

The simulation results show that, to obtain a temperature difference at the ends of the heat source exactly equal to the case with 7 microchannels (221 K), in the configuration with 4 microchannels it is necessary to decrease the power to 104 kW. The mass flow rate circulating in the channel is also significantly reduced, reaching about 0.34 kg/s. The fact that the mass flow rate is so low further increases the performance of the thermocline, decreasing the mixing in the volume. In fact, it is noted that the lower half of the volume is at an almost homogeneous temperature. In the upper part of the storage there is a large gradient, which allows for a fairly high temperature in the upper area. The two curves, unlike the previous case, do not intersect, since the power in the two simulations is different. In conclusion, it is noted that by lowering the input power the performance of the thermocline improves, producing a better temperature stratification.

2.5 Conclusions

In this work, an in-depth study of the operation of a thermocline energy storage for CSP plants was carried out. The study was carried out using the computational fluid dynamics software STAR-CCM+, which allows to simulate the movement of fluids inside the device in a sufficiently precise manner.

The storage tank developed in this thesis is an evolution of a model designed and built by ENEA. In the tank built by ENEA, the stratification of the fluid occurs thanks to a central channel along which the hot fluid rises during the charging phase, while in the charging phase the movement is reversed. One of the most innovative aspects of the models developed in this thesis concerns the implementation of a microwave heating device, which allows to use electrical energy to heat the storage medium.

In this work, numerous simulations of the charging transient with microwave heating were carried out. At first, it was noticed that by imposing a certain constant nominal power, the stratification inside the storage volume was inefficient, resulting in low values of temperature difference and large gradients along the vertical direction. For this reason, it was decided to make some modifications to improve the performance of the thermocline.

The first attempt was carried out by inserting a “fan interface” in the central channel that simulated the operation of an impeller. This method produced disappointing results, with insufficient improvements in temperature stratification.

A second attempt was carried out by replacing a part of the central channel with microchannels of 1 cm diameter each. The introduction of microchannels has the aim of obstructing the passage of the fluid, in order to reduce the circulating flow rate and decrease the recirculation of the fluid. This method produced the desired results. In fact, different configurations were tested with a different number of microchannels in order to cause increasing pressure drops concentrated along the channel. In general, it was noted that by increasing the hydraulic impedance of the channel, the temperature stratification improves, approaching the ideal profile of a thermocline.

The most efficient configuration, considering a heating with a nominal power of 190 kW, was the one with 7 microchannels. In fact, this configuration causes optimal stratification inside the tank, producing an optimal temperature difference to make the most of the operability range of the molten salt.

Therefore, this project has allowed us to achieve two fundamental objectives. The first was the design and implementation of a new device that allows heating the storage medium through microwaves. The second objective concerns the improvement of the performance of the thermocline storage, demonstrating that by increasing the hydraulic impedance of the channel, and therefore, decreasing the circulating flow rate, the temperature stratification in the storage improves significantly.

Appendices

Appendix A

In this section the properties of "Solar salt", a mixture of 60% $NaNO_3$ and 40 % KNO_3 are exposed (Zavoico, 2001), (Ferri R., 2008). Below the table, there are also the temperature-dependent polynomial equations. The reference temperature is set to 273.15 K.

Table 2 - Solar salt properties

T [K]	Density [kg/m3]	Specific heat [J/kgK]	Viscosity [Pa*s]	Thermal conductivity [W/mK]	Enthalpy [J/kg]
533.00	1924.74	1487.69	4.348E-03	0.492	3.81E+05
551.05	1913.26	1490.80	3.818E-03	0.496	4.08E+05
569.10	1901.78	1493.90	3.358E-03	0.499	4.35E+05
587.15	1890.30	1497.01	2.960E-03	0.503	4.62E+05
605.20	1878,82	1500.11	2.621E-03	0.506	4.89E+05
623.25	1867.34	1503.22	2.335E-03	0.510	5.16E+05
641.30	1855.86	1506.32	2.097E-03	0.513	5.43E+05
659.35	1844.38	1509.43	1.901E-03	0.516	5.70E+05
677.40	1832.90	1512.53	1.742E-03	0.520	5.97E+05
695.45	1821.42	1515.64	1.616E-03	0.523	6.25E+05
713.50	1809.94	1518.74	1.516E-03	0.527	6.52E+05
731.55	1798.46	1521.84	1.439E-03	0.530	6.80E+05
749.60	1786.98	1524.95	1.378E-03	0.534	7.07E+05
767.65	1775.50	1528.05	1.328E-03	0.537	7.35E+05
785.70	1764.02	1531.16	1.284E-03	0.540	7.62E+05
803.75	1752.54	1534.26	1.241E-03	0.544	7.90E+05
821.80	1741.06	1537.37	1.194E-03	0.547	8.18E+05
839.85	1729.58	1540.47	1.138E-03	0.551	8.45E+05
857.90	1718.10	1543.58	1.067E-03	0.554	8.73E+05
875.95	1706.62	1546.68	9.760E-04	0.558	9.01E+05
894.00	1695.14	1549.79	8.600E-04	0.561	9.29E+05

Table 3 - Solar salt properties polynomial correlations

Solar Salt (60% $NaNO_3$ and 40 % KNO_3) properties		
Density	$\rho\ [\frac{kg}{m^3}]$	$2090 - 0.636 * T[°C]$
Specific heat	$c_p\ [\frac{J}{kg * K}]$	$1443 + 0.172 * T[°C]$
Viscosity	$\mu\ [Pa * s]$	$(22.714 - 0.120 * T[°C] + 2.281 * 10^{-4} * T[°C]^2 - 1.474 * 10^{-7} * T[°C]^3) * 10^{-3}$
Thermal conductivity	$k\ [\frac{W}{m * K}]$	$0.443 + 1.9 * 10^{-4} * T[°C]$
Enthalpy	$h\ [\frac{J}{kg}]$	$\left[1443 \times T[C] + \frac{0.172 \cdot T[C]^2}{2}\right]_{T_0}^{T}$

Appendix B

In this second appendix, it was decided to make a brief digression regarding the capacity of the thermocline thermal storage considered. This aspect was not considered in the thesis since the capacity was not among the objectives. In fact, in this thesis we tried to study the behaviour of microwave heating, also trying to improve the stratification in the tank. The storage capacity, although one of the most important elements that characterize energy storage, was not among the priorities, given the prototypal nature of the storage tank considered. In the following, a summary table of the state of the storage tank is shown when full charge is reached. Full charge is considered when the upper layer of the tank reaches the temperature of 550 °C (823 K). The total volume of the tank is about 3.78 m^3. From the table it is noted that in the configurations in which the stratification is better (i.e., those in which the number of microchannels is lower), the energy and exergy are lower. This aspect, although it may seem counterintuitive, is reasonable since both energy and exergy strongly depend on the average temperature in the domain. Therefore, if the temperature stratification is lower, also the lower layers of the tank increase their temperature more. So, the lower the level of stratification, the higher is the charging time and the total amount of energy introduced. The storage capacity varies between 540 kWh in the case where the stratification is optimal (7 microchannels) to 775 kWh in the case where the temperature is uniform inside the tank. The charging time varies between just under three hours to just over four hours. The exergy ratio, as expected, is higher in the cases where the stratification is more accentuated.

Table 4 - Additional data

Configuration	Average temperature [K]	Capacity [kWh]	Charging time [min]	Total energy [kWh]	Total exergy [kWh]	Exergy Ratio [-]
7 microch. ΔT=221 K; 0.60 kg/s; 190 kW	744	539	170	1358	545	1.002686
13 microch. ΔT=157 K; 0.82 kg/s; 190 kW	767	608	192	1427	588	1.001282
19 microch. ΔT=120 K; 1.01 kg/s; 190 kW	773	626	198	1445	598	1.000767
25 microch. ΔT=102 K; 1.20 kg/s; 190 kW	782	652	206	1471	615	1.000528
No microch. ΔT=34 K; 3.70 kg/s; 190 kW	807	728	230	1547	663	1.000074
Fully mixed ΔT=0 K; 0 kg/s; 190 kW	823	774	244	1593	693	1

References

A., Barletta. 2022. The Boussinesq approximation for buoyant flows. *Mechanics Research Communications*. 2022.

Alonzo-García A., del Carmen Gutiérrez-Torres C., Jiménez-Bernal, J. A. 2016. Computational fluid dynamics in turbulent flow applications. *Numerical Simulation-From Brain Imaging to Turbulent Flows*. 2016.

Barletta, A. 2022. The Boussinesq approximation for buoyant flows. *Mechanics Research Communications*. 2022.

Bauer, T., Odenthal, C., Bonk, A. 2021. Molten salt storage for power generation. *Chemie Ingenieur Technik*. 2021.

Cagnoli M., Petroni G., Russo V., Zanino R. 2023. *LA 1.12 Ibridizzazione del CSP con altre tecnologie energetiche rinnovabili*. 2023.

Cagnoli, M., Gaggioli, W., Liberatore, R., Russo, V., Zanino, R. 2023. CFD modelling of an indirect thermocline energy storage prototype for CSP applications. *Solar Energy*. 2023.

California Independent System Operator. 2012. Fast Facts: What the Duck Curve Tells us About Managing a Green Grid. [Online] 2012. [Cited: 03 10 2024.] https://www.caiso.com/Documents/FlexibleResourcesHelpRenewables_FastFacts.pdf.

Dincer, I., Rosen, M. A. 2002. *Thermal Energy Storage: Systems and Applications*. 2002.

ESMAP. 2024. Global Solar Atlas. [Online] 2024. [Cited: 09 10 2024.] https://globalsolaratlas.info/.

Ferri R., Cammi A., Mazzei, D. 2008. Molten salt mixture properties in RELAP5 code for thermodynamic solar applications. *International Journal of Thermal Sciences*. 2008.

Gaggioli W., Liberatore R., Di Ascenzi P., Mazzei D., Russo, V. 2020. Experimental test of characterization of an innovative thermal energy storage system based on low melting molten salt thermocline tank integrated with an oil exchanger. *AIP Conference Proceedings*. 2020, Vol. 2303, 1.

Günther M., Eickhoff M., Khalil T., Meyer-Grünefeldt M. 2011. *Advanced CSP Teaching Materials*. 2011.

IEA. 2023. *Net Zero Roadmap: A Global Pathway to Keep the 1.5 °C Goal in Reach*. 2023.

Incropera F. P., DeWitt D. P., Bergman T. L., Lavine, A. S. 1996. *Fundamentals of heat and mass transfer*. New York : Wiley, 1996.

IRENA. 2024. irena.org. [Online] 2024. [Cited: 31 07 2024.] https://www.irena.org/Energy-Transition/Technology/Solar-energy.

Joseph, I. O. 2017. Microwave heating in food processing. *BAOJ Nutrition*. 2017.

Kalaiselvam S., Parameshwaran R. 2014. *Thermal energy storage technologies for sustainability: systems design, assessment and applications*. s.l. : Elsevier, 2014.

Lantelme, F., Groult, H. 2013. *Molten salts chemistry: from lab to applications*. s.l. : Newnes, 2013.

Lappa, M. 2022. Incompressible flows and the Boussinesq approximation: 50 years of CFD. *Comptes Rendus. Mecanique*. 2022.

Lovegrove K., Stein W. 2012. *Concentrating Solar Power Technology Principles, Developments and Applications*. 2012.

Munson B. R., Young D. F., Okiishi, T. H. 1995. *Fundamentals of fluid mechanics*. s.l. : Oceanographic Literature Review, 1995.

Pacheco, J. E., Showalter, S. K., Kolb, W. J. 2002. Development of a molten-salt thermocline thermal storage system for parabolic trough plants. *J. Sol. Energy Eng*. 2002.

Ratnu S. S., Manu K. V. 2021. Three-Dimensional Thermocline Dynamics in Thermal Storage Tanks. *Journal of Applied Fluid Mechanics*. 2021.

Rodríguez-García M. M., Bayón R., Alonso E., Rojas E. 2023. Experimental and theoretical investigation on using microwaves for storing electricity in a thermal energy storage medium. *AIP Conference Proceedings*. 2023.

Russo V., Mazzei D., Liberatore, R. 2018. Thermal energy storage with integrated heat exchangers using stratified molten salt system for 1 MWe CSP. *AIP Conference Proceedings*. 2018, Vol. 2033, 1.

Sobieski W., Trykozko, A. 2014. Darcy's and Forchheimer's laws in practice. Part 1. The experiment. *Technical Sciences/University of Warmia and Mazury in Olsztyn*. 2014.

Terna. 2024. terna.it. [Online] 2024. [Cited: 11 10 2024.] https://www.terna.it/it/sistema-elettrico/transparency-report.

Venkatakrishnan V., Mavriplis D. J. 1996. Implicit method for the computation of unsteady flows on unstructured grids. *Journal of Computational Physics*. 1996.

World Bank. 2021. *Concentrating SolarPower: Clean Power on Demand 24/7*. 2021.

Zanino R., Cagnoli M., Pellegrino I. 2020. Thermal-Fluid Dynamic Modelling of a Thermocline Storage System for CSP Applications. 2020.

Zavoico, A. B. 2001. *Solar Power Tower: Design Basis Document*. 2001.